Electron Impact Excitation of Polarised Sodium and Potassium

By

Muhammad Abdul-Hakim Bukhari
MSc (Ohio University, 1982)

A thesis submitted to the University of Stirling
for the degree of
Doctor of Philosophy

Unit of Atomic and Molecular Physics
University of Stirling
Stirling FK9 4LA

April, 1991

ABSTRACT

A beam of unpolarised electrons is crossed at right angles with a beam of partially polarised sodium or potassium atoms (degree of polarisation P_A = 21%).The resonance radiation from excited $^2P_{3/2,1/2}$ states is observed in a direction perpendicular to both beams, and the Stokes parameters P_1, P_2 and P_3 of the emitted photons are measured,

$$P_1 = \frac{I(0°)-I(90°)}{I(0°)+I(90°)}, \quad P_2 = \frac{I(45°)-I(135°)}{I(45°)+I(135°)}, \quad P_3 = \frac{I(RHC)-I(LHC)}{I(RHC)+I(LHC)}$$

where 0°, 45°, 90° and 135° corresponds to the polariser angle measured from the electron beam direction and RHC, LHC to right and left hand circular polarisation in the spectroscopic definition.Because of reflection symmetries, only P_1 is expected to be non-zero for unpolarised atoms. If polarised atoms are used with their spins parallel to the direction of the observed photons, P_3 should also become non-zero (in addition to P_1) while P_2 remains zero. Such an experiment was originally proposed by Kleinpoppen, Phys. Rev. A3, 2015 (1971).

We report here an independent measurement on the neutral sodium NaI ($3^2P_{3/2,1/2} - 3^2S_{1/2}$) transition (λ = 589.0, 589.6 nm) and present new results for the neutral potassium KI ($5^2P_{3/2,1/2} - 4^2S_{1/2}$) transition ($\lambda$ = 404.4, 404.7nm). The sodium results show close similarities to the work done by S. Osimitsch, Diplomarbeit Universität Bielefeld (1983) and Jitschin *et al* J. Phys. B 17 1899 (1984) especially for P_1 and P_2. The potassium results for P_2 agree well with the theoretical prediction of zero and the results for P_1 show

close similarities to those of sodium results at high and intermediate energies, while at low energy especially close to threshold they differ . The threshold polarisation (P_3) in the case of potassium is about 10%. Our P_3 values for sodium are somewhat higher than the results of Osimitsch (1983) and Jitschin *et al* (1984) and in very close agreement with the theoretical work done by Moores and Norcross, J. Phys. B 5, 1482 (1972) and Kennedy *et al*, J. Phys. B 10 3759 (1977).The trend of P_3 for potassium is similar to that of sodium in such a way that it is low at low energy and increases in value as the energy increases, until it reaches a limit of 17% at high energy. The circular polarisation, P_3, depends on the particular interaction processes which took place. At low energy, the three interaction channels, the exchange, the direct and the interference interaction are comparable and this will explain the low value of P_3 at low energy due to spin flips of the electron of the atom in the exchange processes. At high energy the circular polarisation P_3 is high which indicates that the exchange processes are minimal.

ACKNOWLEDGEMENTS

When I started writing my thesis, I found it quite imperative to show my appreciation for those who made this work possible. For those who are not mentioned in this acknowledgement, I offer my apology and ask their forgiveness.

The one I would like to thank most is my principal supervisor Professor H. Kleinpoppen for giving me the chance to do this kind of research and for his constant help and explanation of the experiment and for his constant encouragement.

I would like also to extend my thanks to my supervisor Dr Alan Duncan for the help he offered to me and also for reading the manuscript of the thesis.

I would like also to thank Professor Trainer (Deputy Principal) for re-admitting me to the University.

Special thanks and deepest respect are due to Dr Jurgen Beyer without whose constant help and suggestions this work would not have been completed.

My thanks also are extended to the two capable technicians, A. J. Duncan and A. D. Sherman for drawing and machining part of the apparatus used for the experiment and their readily available technical assistance.

My appreciation also extend to the Government of Saudi Arabia, who sponsored me for the whole period I stayed at Stirling University.

Finally I would like to thank my wife and family without whose support the task to do research in Stirling would not have been easy.

TABLE OF CONTENTS

CHAPTER I

1 Introduction

The alkali metal atoms such as sodium and potassium, are composed of a single electron outside a core of completely filled electron shells. In the ground state of an alkali metal atom, the outer electron is in the nS state with n = 3 for sodium and n = 4 for potassium. The alkali metal atom is considered to be excited if the outer electron is found to be in the 3P or any higher state for sodium or in the 4P or any higher state for potassium.

The electron impact nS - nP excitation of alkali metal atoms has been the subject of numerous experimental and theoretical investigations since about 1930. The work done before 1968 was reviewed by Moisewitch and Smith (1968 and 1969). The work done between 1968 and 1978 is been covered by Bransden and McDowell (1977 and 1978).

There are three methods of finding the total cross section for excitation. The first method suits the short-lived states. In this method the electon beam collides with the atom in a collision chamber containing the gas under study. Light of the particular wavelength from the collision chamber is then collected at right angles to the electron beam. In the beginning of this century this light was recorded on a photographic plate and the intensity of each

line bears information about the total cross section of that state. Since the invention of the photomultiplier, a more direct relationship is established between the observed light output and the electron excitation cross section.

The second method is suitable for states with a long life time . When a metal surface is bombarded by a beam of metastable atoms , the ejected electron bears information about the state of the metastable atom .

The third method depends on the fact that when an electron collides with an atom it loses energy. Energy loss spectra can be obtained and hence the total cross section for the excitation can be determind .

Different methods have been used in calculating the total cross section for nS - nP excitation of alkali metal atoms and other elements. The basic characteristic of these cross sections is that the highest values are found in the neigbourhood of the excitation threshold due to the strong coupling between the initial and final states of the resonance transition ns - np,as seen in figure 1,taken from

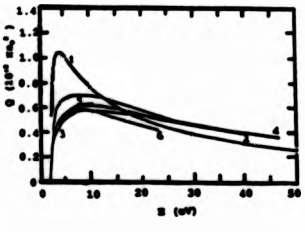

Fig.1 Total cross sections for the 3s-3p excitation of sodium. Curve 1: first Born approximation (Karule and Peterkop, 1965). Curve 2: modified Bethe approximation (Seaton, 1955). Curve 3: impact parameter method (Seaton, 1962). Curve 4:unitarized Born approximation (Salmona and Seaton, 1961). Curve 5: resonance distortion method (Lane and Lin, 1964). Curve 6: 3s-3p close coupling approximation neglecting exchange (Barnes, Lane, and Lin, 1965).

B. Moiseiwitsch and S. Smith(1968). Experimentally , Hafner *et al* (1965) have measured the polarisation of sodium D lines and found that it decreases monotonically with energy from about 15% at threshold as seen in figure 2 .

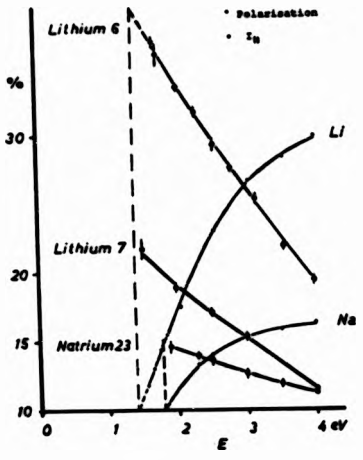

Fig. 2 The excitation function and the polarisation of the first resonance line of ^{23}NaI(Hafner et. al 1965).

Apart from the result given by Hafner *et al* (1965) the work on sodium and potassium reviewed by Moisewitch and Smith (1968) has been carried out in static vapour rather than with beams. Later on many papers appeared using a crossed beam technique to study sodium and potassium. Kennedy *et al* (1977) used the experimental and the theoretical work of the total cross section for excitation of the first resonance line of sodium and potassium and compared it with the theoretical work done by him using the unitarised distorted-wave polarised-orbital model as seen in figure 3 and 4, respectively .

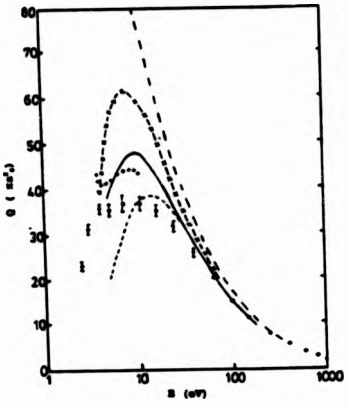

Fig.3.Integrated(total) cross section (πa_o^2) for the first resonance transition of NaI to 1keV. Experimental results:• Enemark and Gallagher (1972); x-x-x Zapesochnyi *et al* (1975). Theoretical results: —.—.— FBA (Walters 1973);- - - Glauber (Walters,1973); ....McCavert and Rudge(1972);———UNWPO II (Kennedy,1977).

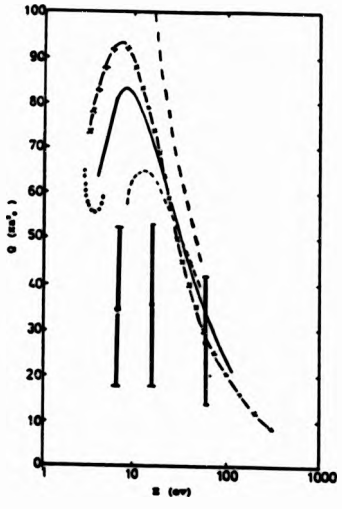

Figure 4.Integrated (total) cross section (πa_o^2) for the first resonance transition of KI to 1keV. Experimental results:o William and Trajmar (1977); x-x-x Zapesochnyi *et al* (1975). Theoretical results: —.—.— FBA (Walters 1973);----Glauber (Walters);....McCavert and Rudge(1972);———UNWPO II (Kennedy,1977).

Heddle and Gallagher (1989) wrote a comprehensive review on

all the experimental work which has been carried out to find the optical excitation functions for sodium and potassium and other elements. This review provides a critical reports of the experimental results . From this review we borrow figure 5 and 6 for sodium and potassium, respectively. Also from Chen and Gallagher (1978) we take figure 7 which summarises most of the theoretical work done to calculate the optical excitation cross section for the resonance transition 4S - 4P for potassium compared to the experimental work. In the time between the appearance of the comprehensive reviews by Moiseiwitch and Smith (1968) and by Heddle and Gallagher (1989) many papers appeared in which the total cross sections for the excitation of sodium and potassium were determined. The measurement of the total excitation cross section is essential because, when atoms are excited by unpolarised electrons and the light emitted

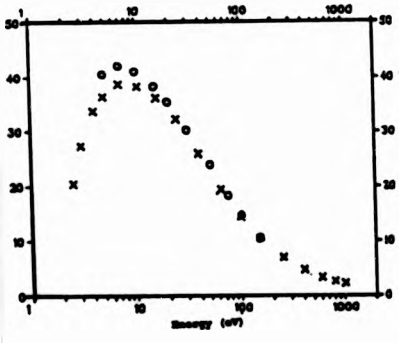

Fig 5. Excitation function of the D lines of sodium: (X) Enemark and Gallagher (1972); (O) Phelps and Lin (1981).

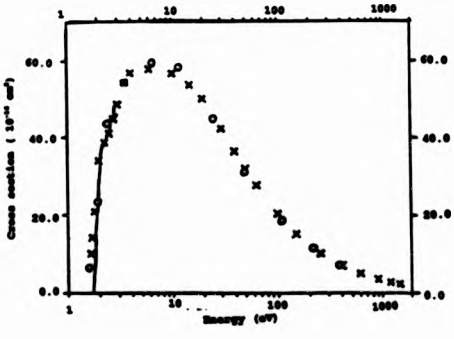

Fig. 6. Excitation function of the resonance doublet of potassium: (X) Chen and Gallagher (1978); (O) Phelps *et al.* (1979); (___) Papp *et al.* (1983).

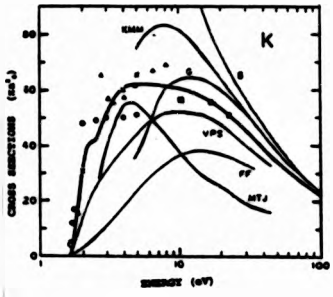

Fig. 7. Normalized optical excitation cross section for the resonance transition of KI compared with theoretical calculations . The excitation cross section of KI have been calculated by Vainshtein *et al.(1965)*,. (first Born and VPS), Green and Williamson(1974) (first Born, Bethe and Ochkur), McCarvert and Rudge(1972), (truncated Born-Oppenheimer approximation), Felden and Felden(1973), (correlation model), Walters(1973), (Glauber approximation), Kennedy *et al.(1977)*,. (unitarized-wave-polarized-orbital model (ODWPO), and Mathur *et al.(1969)*, (classical impulse approximation). There are also independent close-coupling calculation including exchange by Karule and Peterkop, the three-state (4S-4P-3D) coupling including exchange by Moores(1976), and the 15-state coupling without exchange by Korff and Lin(1973).

in the subsequent decay is observed without detecting the scattered electrons, then the polarisation properties of the emitted radiation will depend on two parameters, the total cross section and the atomic alignment (Bartschat, 1982 and Percival & Seaton, 1958). If we choose , in such a measurement, the incoming electron beam to be in the -OY direction, then the radiation emitted may be considered to be due to electric dipoles in OY direction and two other equal dipoles in the OX and OZ directions. Using unpolarised electrons and unpolarised atoms, the following papers reported measurements of the total excitation cross section for sodium and potassium: Enemark and Gallagher (1972) measured the total cross section for excitation and found that, at low energy, from threshold up to 5 eV , the normalized cross section and the polarisation were in excellent agreement with the close coupling calculations.

Another comprehensive work was done by Phelps and Lin (1981) on sodium, in which they measured the total optical cross sections for 14 states. Beside the work done for sodium, Kennedy and McDowell (1977) calculated the total cross section for excitation of the resonance transition in LiI, NaI and KI using the distorted-wave polarised-orbital approximation. A similar study on potassium was carried out by Phelps *et al.* (1979), from which we borrow figure 8, the total optical excitation cross section to excite potassium from 4s to np (4,5,..,8).It may be noted that theoretical calculations directly provide cross sections of excited states while experimental cross sections may be drived from the intensity and the polarisation of the a particular fluorescence transition from the excited state in question and this optical transition intensity is often shown on its on as for example in Fig 8.State and line cross sections are identical for the first excited state ,e.g for the 3P state of Na and 4P state of K . for higher excited states several decay channels exist and the appropriat branching ratios have to be taken into account if the state cross section is to be derived from fluorescence intensity measurement.

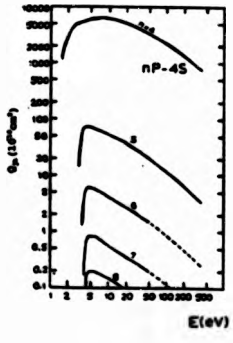

Fig.8 Experimental optical excitation functions of potassium for the principal series .Solid lines indicate experimental measurements; dashed lines represent extrapolations,Phelps *et al.* (1979).

In the previous pages we have summarized the total cross sections and the total optical excitation cross sections when both colliding partners are unpolarised. To clarify the behavior better we should know the different channels of interaction for which the partial cross section can be used to calculate the final cross section. The different interaction channels involved in the scattering process of unpolarised parteners are given in table (1).

Table 1

Electron scattering by a spin ½ particle

Component of electron spin along magnetic field				
Before collision		After collision		Channel of Interaction
Atomic electron	Incident electron	Atomic electron	Scattered electron	
½	½	½	½	interference
½	−½	½	−½	direct
½	−½	−½	½	exchange
−½	½	½	−½	exchange
−½	½	−½	½	direct
−½	−½	−½	−½	interference

A first step towards calculating the contribution of each interaction channel to the total cross section is to make one of the collisional partners polarised, in our case the atomic beam. The different interaction channels are then given by:

a) $e(\uparrow\downarrow) + A(\uparrow) \rightarrow e(\uparrow) + A^*(\uparrow)$ interference (I-1)

b) $\rightarrow e(\downarrow) + A^*(\uparrow)$ direct (I-2)

c) $\rightarrow e(\uparrow) + A^*(\downarrow)$ exchange (I-3)

where the arrows indicate the spin direction , $e(\uparrow\downarrow)$ stands for unpolarised electron, $A(\uparrow)$ for polarised atom and A* for the excited atom.

We detect the photons along the OZ-axis with the atomic beam in the OX- direction. If the polarisation vector of the atoms is along OZ, then this kind of experiment is no longer cylindrically symmetric about the electron beam but defines a sense of rotation in the XY-plane about the atomic polarisation vector. As a consequence of this the degree of circular polarisation of the observed decay light is no longer zero (Bartschat and Blum, 1982). Such an experiment using polarised partners and investigating the properties of the light was originally proposed by Kleinpoppen (1971). For impact energies large compared with the excitation threshold, the exchange interaction becomes negligible, whereas close to threshold all reaction channels may be of comparable magnitude. Information about the exchange interaction can be obtained directly if the spin of the atomic collision partner is known prior to and after the interaction. The exchange cross section for the scattering of low-energy electrons by potassium has been determined by Rubin *et al.* (1960). Under the action of spin-exchange, polarised electrons were obtained from scattering on polarised potassium atoms(Campbell *et al.* 1971). In that paper the spin exchange cross-section is high at threshold and decreases very rapidly as the energy increases. For

sodium the interference between the direct and exchange interactions has been determined in a study involving polarised electrons and polarised sodium atoms (Shröder, 1982) and Baum *et al* (1982) . Jitschin *et al* (1984) reported the first measurement of electron impact excitation of spin-polarised sodium atoms with a polarisation analysis of the fluorescence light.

The present experiment was a crossed-beam arrangment in which an unpolarised electron beam crossed a partially-polarised sodium or potassium beam. The work of Jitschin *et al* . (1984) and Osimitsch (1983) on the fluorescence light emitted by sodium excited to the 3P state is confirmed and for the first time a full polarisation analysis is carried out for the 5P - 4S fluorescence light emitted as a result of 5P state excitation on partially polarised potassium.

In chapter II a brief theoretical discussion of the fluorescence analysis is given. In chapter III, we describe the overall apparatus and details of the experiment and in chapter IV we explain the results obtained for sodium and potassium. In chapter V we make concluding remarks.

CHAPTER II

2 Theoretical Points

In this theoretical presentation we follow the work done by Jitschin *et al* (1984). In this treatment the atomic beam can be considered as a mixture of states such that the density matrix which represents this mixture can be expanded in a series of state multipoles $\langle T^{K}_{KQ} \rangle$ of different rank K, i.e. monopoles, dipoles, etc (Blum, 1981). In all formulae we are using the direction of the magnetic field, which is also the direction of the spin of the outer electron of the atom, as our quantisation axis (polarization frame).

2.1 Preparation of a State-Selected Na and K Beam

A hexapole magnet was used to polarise the atomic beam. Our measured polarisation of the atomic beam in low magnetic field is about 21%(see 3.3.4 and 3.3.5). In this low magnetic field the atomic beam can be described by an incoherent set of atoms being in different FM_F hyperfine states. The density matrix of such a beam is diagonal. The elements of the density matrix are the occupation numbers $W(FM_F)$. The density matrix can be expanded into a series of state multipoles $\langle T(F)^{K}_{KQ} \rangle_{F,F}$ which are actually the set of $(2F + 1)^2$ multipole operators , pertaining to the orientation of particles having angular momentum F. Each operator $T(F)_{KQ}$ is represented by a $(2F + 1)x(2F + 1)$

matrix. The multipole operators are conveniently chosen in tensorial form $T(F)_{K\,Q}$ so that they transform under coordinate rotations like the spherical harmonics (Druckarev, 1987).

Y_{KQ}, $Q = -K \ldots\ldots\ldots +K$ and $K = 0, \ldots\ldots 2F$.

The state multipole $\langle T(F)^{\dagger}_{K\,Q} \rangle$ is given by;

$$\langle T(F)^{\dagger}_{K\,Q} \rangle = \sum_{M_1 M_2} (-1)^{F-M_2} (FM_1, F - M_2 | K, Q) \delta_{M_1 M_2} W(FM_1) \qquad \text{(II-1)}$$

Here (:|:) is the Clebsch - Gordan Coefficient.

In collision experiments one is interested in electronic and nuclear parameters separately. The corresponding representation by the uncoupled state multipoles is

$\langle T(S)^{\dagger}_{K\,Q} \times T(I)^{\dagger}_{K\,Q} \rangle$ (Blum 1981 (B7)).

$$\langle T(S)^{\dagger}_{K\,Q} \times T(I)^{\dagger}_{K\,Q} \rangle =$$

$$\sum_{FK_1Q_1} (2F+1)\,[(2K_1+1)(2K_2+1)]^{\frac{1}{2}} (K_1Q_1, K_2Q_2 | K, Q)$$

$$\times \begin{vmatrix} K_1 & K_2 & K \\ S & I & F \\ S & I & F \end{vmatrix} \langle T(F)^{\dagger}_{K\,Q} \rangle \qquad \text{(II-2)}$$

where $\begin{vmatrix} . & . & . \\ . & . & . \\ . & . & . \end{vmatrix}$ is a 9-j symbol; and I is the nuclear spin.

A straight forward calculation shows that the electronic spin polarisation P_S and the nuclear vector polarisation P_I can be expressed by these multipoles:

$$P_s = \langle T(S)^{\dagger}_{10} \times T(I)^{\dagger}_{00} \rangle \langle T(S)^{\dagger}_{00} \times T(I)^{\dagger}_{00} \rangle^{-1} \qquad \text{(II-3)}$$

$$P_z = (3/9)^{1/2} \langle T(S)^{\dagger}_{00} \times T(I)^{\dagger}_{10} \rangle \langle T(S)^{\dagger}_{00} \times T(I)^{\dagger}_{00} \rangle^{-1}. \qquad \text{(II-4)}$$

In equation (II-1) the occupation number $W(FM_F)$ is given for the ground state of sodium and potassium atoms by,

$$W(FM_F) = (1/8)(1 \pm s) \qquad \text{(II-5)}$$

where s is the selectivity of the hexapole magnet and the (-) is applicable for F = 1 and M_F = -1, 0, +1 and also for F = 2 and M_F = -2,while the (+) is applicable for F = 2 and M_F = -1, 0, +1, +2, . On the assumption that the selectivity (s) of the hexapole magnet is 0.7 (Hils,et.al. 1981), table (1) gives the occupation number $W(FM_F)$ of sodium and potassium ground state atoms.

Table 1

State F	M_F	Magnet state selection $W(FM_F)$ of Na and K
1	-1	0.0375
1	0	0.0375
1	+1	0.0375
2	-2	0.0375
2	-1	0.2125
2	0	0.2125
2	+1	0.2125
2	+2	0.2125

2.2 Collision Induced S-P Excitation

We adopt what was suggested by Blum and Kleinpoppen (1979) that, in the excitation process, all the angular momenta are decoupled. In a collision experiment the scattering plane is defined by the direction of the incoming electrons and the direction of the outgoing electrons. In the ground state the angular shape of the S state is isotropic, while the excited P states in general exhibit anisotropy as shown in figure (9)

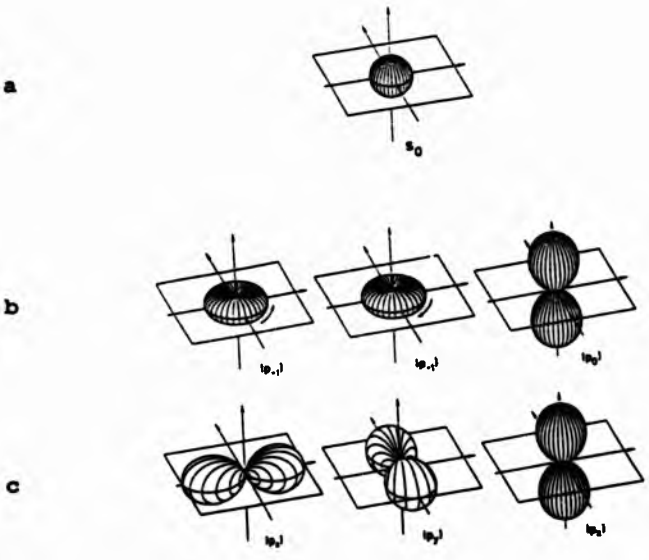

Figure (9) shows the charge cloud for the state S (m=0) Figures 9b and 9c show the charge cloud for the state 3P with magnetic quantum number M_L = +1, -1, and 0 (b) in the atomic physics basis and (9c) in molecular physics basis. Andersen (1988).

In non-coincident experiments in which we count photons

regardless of the scattered electron direction, so that the observed quantity is integrated over all scattering angles of the electrons, one does not obtain information on the differential cross section but rather on the integral cross sections for excitation of the 3P state (Moores and Norcross 1972). Then , with $M_i = M$, we obtain

$$Q_M = \tfrac{1}{4}\{D_M + E_M + I_M\} \qquad \text{(II-6)}$$

where Q_M is the total cross section and ,

$$D_M = (k_f/k_i)\int |f_M|^2 d\Omega \qquad \text{(a)}$$

$$E_M = (k_f/k_i)\int |g_M|^2 d\Omega \qquad \text{(b)} \qquad \text{(II-7)}$$

and $$I_M = (k_f/k_i)\int |f_M - g_M|^2 d\Omega \qquad \text{(c)}$$

where k^2_f and k^2_i are the final and initial electron energies. f_M and g_M are the direct and exchange amplitude and Ω is the solid angle.

In a crossed beam electron atom scattering experiment,in which the electron beam is in the -OY-direction and the atomic beam in the OX-direction, the photon detector in the OZ-direction, the experiment will have cylindrical symmetry about the Y-direction if the two colliding partners are unpolarised . But now , if the atomic beam is polarised along the Z-direction , the collision geometry loses its axis of symmetry . In this case the polarisation P of the atom defines a sense of rotation in the XY-plane and the

geometry of the experiment will have only reflection symmetry in the XY-plane . In such a geometry P_2 (the linear polarisation Stokes parameter corresponding to polariser angles 45° and 135° with respect to -y) is not necessarily zero.

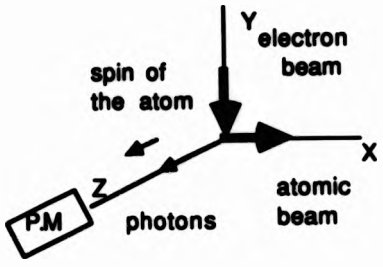

Fig (10) Geometry of the experiment at the interaction region.

So, for sodium which in its excited state exhibits anisotropy that can be described by a state multipole of rank larger than zero , the only state multipoles which do not vanish due to symmetry are $\langle \bar{T}(L)^{\dagger}_{00} \rangle$ and $\langle \bar{T}(L)^{\dagger}_{20} \rangle$. Here the impact axis is considered to be our quantization axis which is indicated by a bar on top of T. These integrated state multipoles are related to the excitation cross sections Q_0 and Q_1 of the magnetic substates $M_L = 0$ and $M_L = \pm 1$ respectively by

$$\langle \bar{T}(L)^{\dagger}_{00} \rangle = (1/3)^{1/2}(2Q_1 + Q_0) \qquad \text{(II-8)}$$

$$\langle \bar{T}(L)^{\dagger}_{20} \rangle = (2/3)^{1/2}\ (Q_1 - Q_0) \qquad \text{(II-9)}$$

If we rotate our quantization axis through 90° and make it parallel to the spin polarization axis Z where we placed our photodetector (instead of having it along the electron impact axis (Edmonds, 1957)), the state multipoles in the

new form can be obtained as

$$< T(L)^{\dagger}_{00} > = < \hat{T}(L)^{\dagger}_{00} > \quad a$$

$$< T(L)^{\dagger}_{2\pm2} > = (3/8)^{1/2} < \hat{T}(L)^{\dagger}_{20} > \quad b$$

$$< T(L)^{\dagger}_{2\pm1} > = 0 \quad c \qquad \text{(II-10)}$$

$$\text{and } < T(L)^{\dagger}_{20} > = -\tfrac{1}{2} < \hat{T}(L)^{\dagger}_{20} > \quad d$$

From the previous discussion for electron interaction with polarised atoms we found that there are three channels in which this interaction can happen; direct (D), exchange (E) and mixed (I) interaction. Each interaction can be represented by the state multipoles $< T^{D}(L)^{\dagger}_{K Q}{}_{L L} >$, $< T^{E}(L)^{\dagger}_{K Q}{}_{L L} >$ and $< T^{I}(L)^{\dagger}_{K Q}{}_{L L} >$ which can be calculated if one knows the corresponding cross sections for the magnetic substates.

The electron spin in a collision experiment is conserved in the direct and the mixed excitation channel while a spin flip occurs in the exchange channel (Burke and Schey 1962 and Norcross 1972). On the assumption that the nuclear spin is not affected by the collision process, the complete description of the excited state immediately after the collision in terms of the uncoupled state multipoles is given by Jitschin *et al.* (1984) as, $< T(L)^{\dagger}_{K Q}{}_{L L} \times T(S)^{\dagger}_{K Q}{}_{S S} \times T(I)^{\dagger}_{K Q}{}_{I I} >$ so,

$$< T(L)^{\dagger}_{K Q}{}_{L L} \times T(S)^{\dagger}_{K Q}{}_{S S} \times T(I)^{\dagger}_{K Q}{}_{I I} >$$

$$= \tfrac{1}{4} < T^{D}(L)^{\dagger}_{K Q}{}_{L L} + T^{I}(L)^{\dagger}_{K Q}{}_{L L} > < T(S)^{\dagger}_{K Q}{}_{S S} \times T(I)^{\dagger}_{K Q}{}_{I I} >$$

$$+ \tfrac{1}{4} < T^{E}(L)^{\dagger}_{K Q}{}_{L L} > < \pm T(S)^{\dagger}_{K Q}{}_{S S} \times T(I)^{\dagger}_{K Q}{}_{I I} >$$

$$= \tfrac{1}{4} < T^{D}(L)^{\dagger}_{K Q}{}_{L L} \pm T^{E}(L)^{\dagger}_{K Q}{}_{L L} + T^{I}(L)^{\dagger}_{K Q}{}_{L L} > < T(S)^{\dagger}_{K Q}{}_{S S} \times T(I)^{\dagger}_{K Q}{}_{I I} > \qquad \text{(II-11)}$$

The state multipoles $\langle T(S)^{\dagger}_{K_s 0} \times T(I)^{\dagger}_{K_s 0} \rangle$ are the same as for the ground state and the ± signs apply for $K_s = 0$ and $K_s = 1$, respectively, for sodium.

2.3 Fine and Hyperfine Interaction of the Excited state

For alkali metal atoms the outer electron rotates about the nucleus with an orbital angular momentum (L) and the intrinsic (spin) angular momentum (S). The spin -orbit interaction between these causes the fine structure in the atomic spectrum. A further splitting of the spectral line, the hyperfine structure, results from the fact that the atomic nucleus has an angular momentum of its own (I),normally called nuclear spin. Actually ,the splittings of the hyperfine structure for sodium and potassium are large compared to the natural level width ,see figure 49 .In terms of the state multipole language if both electron and nuclear spin are unpolarised then the effect of coupling the fine and the hyperfine structure is to reduce collisionally induced orientation and alignment by a certain factor which depends on the rank of the state multipoles . i.e state multipoles of different angular momentum are mixed, but not state multipoles of different rank . This results in depolarisation of the atomic beam by a certain factor . The depolarisation may be described by depolarisation coefficients G_K where K is the rank. Then

$G_0 = 1 \quad G_1 = 0.390$ and $G_2 = 0.0982$

These values which show that the orientation (rank 1) is less affected than the alignment (rank 2) are taken from

Jitschin et.al.(1984) who took Na3P splitting values from Hertel and Stoll (1977).

When ,in the case of state selected Na atoms ,the atomic electron is polarised and the nucleus is aligned and oriented immediately after the excitation , then the state multipoles of different rank can mix by the effect of fine and hyperfine coupling. The polarisation properties of the emitted fluorescence light are determined by the spatial state multipoles $\langle T(1)^{\dagger}_{k_1 q_1} \rangle$ averaged over the decay time (this spatial state multipole is denoted by lower case indices). Also Jitschin et. al. (1984) obtained the time-averaged perturbed multipoles $\langle T(1)^{\dagger}_{k_1 q_1} \rangle$ as a weighted sum over the multipoles $\langle T(L)^{\dagger}_{k_L 0} \rangle \times T(S)^{\dagger}_{k_S 0} \times T(I)^{\dagger}_{k_I 0} \rangle$

$$\langle T(1)\dagger_{k_1 q_1}\rangle = [(2S+1)(2I+1)]^{1/2} \langle T(1)^{\dagger}_{k_1 q_1} \times T(S)^{\dagger}_{00} \times T(I)^{\dagger}_{00} \rangle$$

$$= [(2S+1)(2I+1)]^{1/2} \sum_{\substack{K_L Q_L \\ K_S Q_S \\ K_I Q_I}} \langle T(L)^{\dagger}_{k_L 0} \times T(S)^{\dagger}_{k_S 0} \times T(I)^{\dagger}_{k_I 0} \rangle \underline{\underline{G}}^{\substack{Q_L Q_S Q_I q_1 \\ Q_L Q_S Q_I q_1}} \qquad \text{(II-12)}$$

and $\underline{\underline{G}}$ now is given by

$$\underline{\underline{G}}^{\substack{Q_L Q_S Q_I q_1 \\ Q_L Q_S Q_I q_1}} = \sum_{\substack{JF \\ J'F' \\ K_J}} \frac{[(2K_L+1)(2K_S+1)(2K_I+1)(2K_J+1)]^{1/2}}{1+(W_{JF}-W_{J'F'})^2 t^2} (2K_1+1)(2J+1)$$

$$\times (2J'+1)(2F+1)(2F'+1)(K_L Q_L, K_S Q_S | K_J Q_J + Q_S)$$

$$\times \begin{vmatrix} K_L & K_S & K_J \\ L & S & J' \\ L & S & J \end{vmatrix} \begin{vmatrix} K_J & K_I & k_1 \\ J' & I & F' \\ J & I & F \end{vmatrix} \begin{vmatrix} k_1 & 0 & K_1 \\ L & S & J' \\ L & S & J \end{vmatrix} \begin{vmatrix} k_1 & 0 & K_1 \\ J' & I & F' \\ J & I & F \end{vmatrix}$$

(II-13)

Table 2
Perturbation coefficient $\underline{G}$ for Na 3P state needed to calculate (II-12)

K_1	q_1	K_2	Q_2	K_3	Q_3	K_4	Q_4	$\underline{G}^{Q_1Q_2Q_3Q_4}_{q_1q_2q_3q_4}$
0	0	0	0	0	0	0	0	1.000 000
1	0	0	0	0	0	1	0	0.348 480
1	0	0	0	1	0	0	0	0.216 245
1	0	0	0	1	0	2	0	-0.010 709
1	0	2	0	0	0	1	0	-0.011 300
1	0	2	0	0	0	3	0	-0.005 514
1	0	2	0	1	0	0	0	-0.025 826
1	0	2	0	1	0	2	0	-0.053 211
2	0	0	0	0	0	2	0	0.120 754
2	0	0	0	1	0	1	0	0.063 136
2	0	0	0	1	0	3	0	0.008 030
2	0	0	0	1	±1	1	±1	0.031 568
2	0	2	0	0	0	0	0	0.098 207
2	0	2	0	0	0	2	0	0.039 597
2	0	2	0	1	0	1	0	0.021 925
2	0	2	0	1	0	3	0	-0.024 963
2	0	2	0	1	±1	1	±1	-0.007 176
2	2	2	2	0	0	0	0	0.098 207
2	2	2	2	0	0	2	0	-0.039 597
2	2	2	2	1	0	1	0	0.002 260
2	2	2	2	1	0	3	0	0.022 695
2	2	2	2	1	±1	1	±1	-0.006 780

We note that in the case of vanishing hyperfine coupling only the $\underline{G}$ coefficient with $K_i = Q_i = 0$ would survive thus considerably reducing the number of relevant coefficients.

The G and $\underline{G}$ coefficients contain the angular momentum coupling of the excited state as well as electronic and nuclear spin polarisation properties of the excited atoms immediately after the collision. So, the $\underline{G}$ coefficients describe the angular momentum coupling and for that reason it is possible to investigate the influence of electronic and nuclear polarisation on the polarisation of the fluorescence light in more detail.

2.4 Polarisation of the Fluorescence Radiation

The spatial state multipoles $\langle T(1)^{\dagger}_{k_1 q_1} \rangle$ can be used to calculate the Stokes polarisation parameters given by Bartschat *et al* (1981) and applied by Jitschin et. al. (1984),

$$P_1 = \frac{-(3)^{1/2}\langle T(1)^{\dagger}_{22}\rangle}{\langle T(1)^{\dagger}_{00}\rangle + \langle T(1)^{\dagger}_{20}\rangle} \qquad \text{(a)}$$

$$P_2 = 0 \qquad \text{(b)} \qquad \text{(II-14)}$$

$$P_3 = (3/2)^{1/2}\frac{\langle T(1)^{\dagger}_{10}\rangle}{\langle T(1)^{\dagger}_{00}\rangle + \langle T(1)^{\dagger}_{20}\rangle} \qquad \text{(c)}$$

The spatial state multipole given by (II-11) can be used to approximate the formulae (II-14) by expanding the spatial state multipoles $\langle T(1)^{\dagger}_{k_1 q_1} \rangle$ in terms of equation (II-11) and retaining only the terms with largest perturbation coefficient $\underline{G}$, taken from table (II-3)

$$P_1 = (3)^{1/2}\frac{\langle T(1)^{\dagger}_{22}\rangle}{\langle T(1)^{\dagger}_{00}\rangle}$$

$$\approx -(3)^{1/2} \times 0.098 \times \frac{\langle T(L)^{\dagger}_{22} \times T(S)^{\dagger}_{00} \times T(I)^{\dagger}_{00} \rangle}{\langle T(L)^{\dagger}_{00} \times T(S)^{\dagger}_{00} \times T(I)^{\dagger}_{00} \rangle}$$

$$\approx P \qquad (a')$$

$$P_2 = 0 \qquad (b')$$

and

$$P_3 \approx (3/2)^{1/2} \left| \frac{\langle T(1)^{\dagger}_{10} \rangle}{\langle T(1)^{\dagger}_{00} \rangle} \right| \qquad (II\text{-}17)$$

$$= (3/2)^{1/2}(0.348) \times \frac{\langle T(L)^{\dagger}_{00} \times T(S)^{\dagger}_{00} \times T(I)^{\dagger}_{00} \rangle}{\langle T(L)^{\dagger}_{00} \times T(S)^{\dagger}_{00} \times T(I)^{\dagger}_{00} \rangle}$$

$$+ \quad 0.216 \times \frac{\langle T(L)^{\dagger}_{00} \times T(S)^{\dagger}_{00} \times T(I)^{\dagger}_{00} \rangle}{\langle T(L)^{\dagger}_{00} \times T(S)^{\dagger}_{00} \times T(I)^{\dagger}_{00} \rangle} \qquad (c')$$

$$= (27/10)^{1/2} \times 0.348 P_I + (3/2)^{1/2} \times 0.216 P'_e$$

We notice from (II-15) (a'), and (b') that both results are as expected from the theories given by Bartschat *et al* (1981) and Bartschat and Blum (1982) while (II-17)c' which gives the circular polarisation Stokes parameter P_3 depends on two terms. The first term is limited to the nuclear spin polarisation P_I, which depends on the polarisation of the atomic beam, whereas the second term is linked to the electron spin polarisation P'_e of the collisionally excited state and thus bears information on the excitation process.

A numerical example for potassium , prepared by the hexapole, is that the nuclear orientation alone yields a circular light polarisation $P_3 = 0.120$. Taking into account the collisional interaction, we have to consider two limiting cases: firstly spin-conserving direct or interference interaction would give $P_3 = 0.120 + 0.056 =$

0.176 ; secondly only spin-reversing exchange interaction alone would yield $P_s = 0.120 - 0.056 = 0.064$. The first case is generally realised at high collision energies; in contrast the second case is expected to be realised only for differential measurements at certain angles (Moores and Norcross, 1972). All other conditions have to be somewhere in between.

CHAPTER III

3 APPARATUS

3.1 The Vacuum System

An already constructed vacuum system was used to perform the experiment (plate 1). It consists of three chambers. The reason for having three chambers is to accommodate any development in the future, such as using a laser to increase the polarisation of the atomic beam.

The first chamber is called the oven chamber since it accommodates the oven for producing the atomic beam ; the chamber consist of a cylinder of 350 mm diameter and length 650 mm. There are NW-350 flanges one at either end. One flange is bolted to a trolley to provide easy access to the inside of the first chamber. The second flange of the oven chamber is connected to a very small chamber called the laser chamber (the second chamber) which houses the hexapole magnet. There are two rods coming out of the second flange towards the oven chamber on which the oven assembly sits (figure 12 and plate 2).

The second chamber also houses some of the magnetic field coils described later and can be used to admit laser light to optically pump the alkali atoms. The laser chamber is in the form of a cross of 200mm length and width and is connected to the large rectangular scattering chamber. The

dimensions of the scattering chamber are 900mm x 900mm x350mm. There are NW350 flanges on the large faces of the

Plate 1: A photograph of the whole apparatus

chamber, and smaller flanges on the other faces. One whole side of this chamber is formed by a big flange on which a plate is mounted which supports a turntable 670mm in diameter. The flange is bolted to a trolley and the flange, support plate, turntable and all the attached components can be wheeled along the framework to allow easy access to all the components.

As we said, one side of the scattering chamber is connected to the laser chamber and the opposite side of the scattering chamber is connected to a tube. At the end of this tube

sits a Rabi magnet of 100mm length; following this is another tube at the end of which a Langmuir - Taylor detector is mounted. A liquid nitrogen cryogenic pump is situated just behind this detector in order to improve the vacuum condition for the Langmuir -Taylor detector.
All NW350 flanges were sealed by viton O-rings. For the small flanges, the electrical feed throughs and the connection between the tubes, copper O-rings were used to achieve a vacuum seal.

The system was evacuated by two oil diffusion pumps. Differential pumping was achieved in the system. A six inch oil diffusion pump, model 160/700 provided by Edwards, was used to evacuate the oven chamber. The pumping speed of the pump for air is 700 ltr/sec and a pressure of 6×10^{-7} mbar was reached in the oven chamber without any sodium or potassium in the chamber . A typical pressure with hot alkali metal present in the oven was 8×10^{-7} mbar. Another six inch diameter oil diffusion pump (Edwards model 160-150) was used to evacuate the scattering chamber and the tubes. The pumping speed for air for this pump is also 700 ltr/sec. After several days of pumping a pressure of 3×10^{-7} mbar was reached, but the experiment was usually carried out at a pressure of 6×10^{-7} mbar. Only when we measured the polarisation of the atomic beam was liquid nitrogen added to the container located after the Langmuir-Taylor detector. The two diffusion pumps were connected in parallel to a two stage rotary pump (Balzers DUO 35) which can create a backing pressure for the diffusion pump of the order of 4×10^{-2} mbar. The oven and the scattering chambers were isolated from the diffusion pumps by means of electro-

pneumatically operated VAT gate valves model NW-200.

3.2 Cancellation of the magnetic field

The magnetic field which is present in our laboratory is mainly due to the earth's magnetic field but some is due to the electrical trunking of the building, and, inside our chambers, especially the scattering chamber, an extra contribution to the magnetic field comes from the residual magnetism of the stainless steel chamber and other components of the apparatus. To compensate the resultant magnetic field in the interaction region three pairs of coils were used , based on a system of a pair of square coils (Friester, 1966) . The first pair of coils, placed such that its plane is perpendicular to the atomic beam direction cancels the component of the field along that direction . It is rectangular, 790mm x 880mm, with a separation of 440mm . The second pair of coils is placed such that its plane is perpendicular to the photon direction and it cancels the field components along that direction. It is square with a side length equal to 1630mm and a separation of 960mm. The third pair of coils compensates the vertical component , in the direction along the electron beam . This pair of coils has the form of a truncated square with the number of current turns on the shifted side AB (LM) being reduced to half of that on the other three sides (figure 11).To complete the current loop an auxiliary loop ABFE (LMQP) is used were EF(PQ) is placed on the ceiling (floor) to obtain maximum separation from

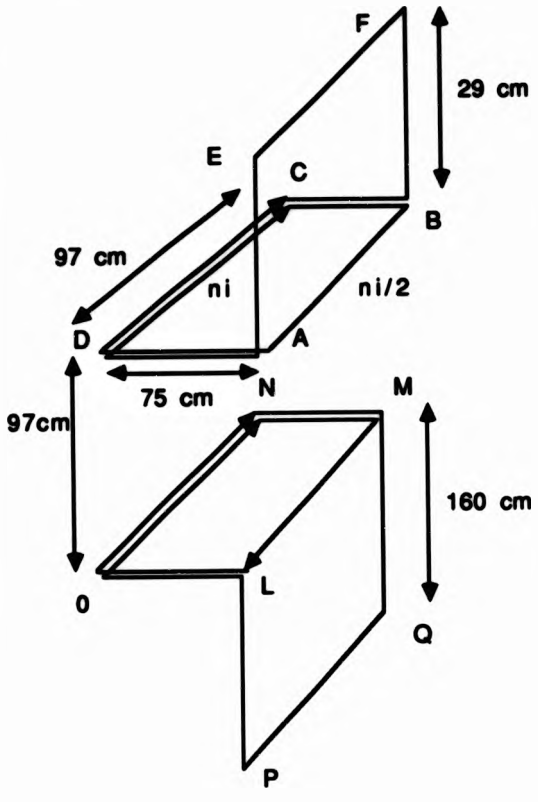

Figure 11. Helmholtz coil system for the vertical component of the magnetic field.

AB(LM) and minimise its effect at the centre. The separation of sides AE and BF (LP and MQ) with reduced current and direction away from the region of interest ensures that the effects on the other components is minimal. All these coils were powered by Farnell stablized power supplies L30B and L30D. After compensating the magnetic field in the interaction region the measured magnetic field

there was in the range of 10 milligauss and up to 35 milligauss along the electron gun.

3.3 THE COMPONENTS OF THE ATOMIC BEAM APPARATUS

3.3.1 The Oven

The oven is designed to evaporate the alkali metals with a reduced dimer population. To do so, the vapour in the hot dissociating region is isolated from the equilibrated liquid - vapour system (Melissa *et al*, 1977) (figure 12 and plate 2).

The hot dissociating region (nozzle) of the oven is connected to the equilibrated liquid - vapour region (the main body), via a tube (interconnecting tube). The inner diameter of the interconnecting tube must be carefully chosen such that no molecular beam collision happens inside it.

The oven is constructed of molybdenum with a nozzle aperture of 1.5mm diameter. The main body can hold four to five 13g pieces of Na. The oven assembly sits on top of three screws which allow the oven to be raised or lowered to the desired position and prevents heating of the base (plate 2). In addition, the whole oven platform can be pushed backward or forward to place it at the desired distance away from the hexapole magnet. The oven can also be rotated about its axis. The main body of the oven was shielded with stainless steel whose function is to reflect back some of the

radiation to the main body.

Two thermometers, made from chromel-alumel, are used for measuring the temperatures of the main body and the nozzle. The first is placed at the bottom of the main body and the second is placed in contact with the nozzle body. The main body is heated with six resistors each of resistance 20Ω (5W). These wire wound resistors are inserted into holes drilled from the bottom into the wall of the main body, while the interconnecting tube and nozzle are heated with thermo-coax wires.

We usually start by heating up the interconnecting tube and the nozzle in order to clear away any residual sodium or potassium metal. Then we commence to heat up the main body of the oven.

Plate 2: The oven assembly inside the oven chamber

A) Nozzle aperture
B) Nozzle
C) Interconnecting tube
D) Thermocoax
E) Main body of the oven
F) Heater for the main body
G) Base for the oven
L) Screw
M) Water cooled condenser
N) Heated aperture.

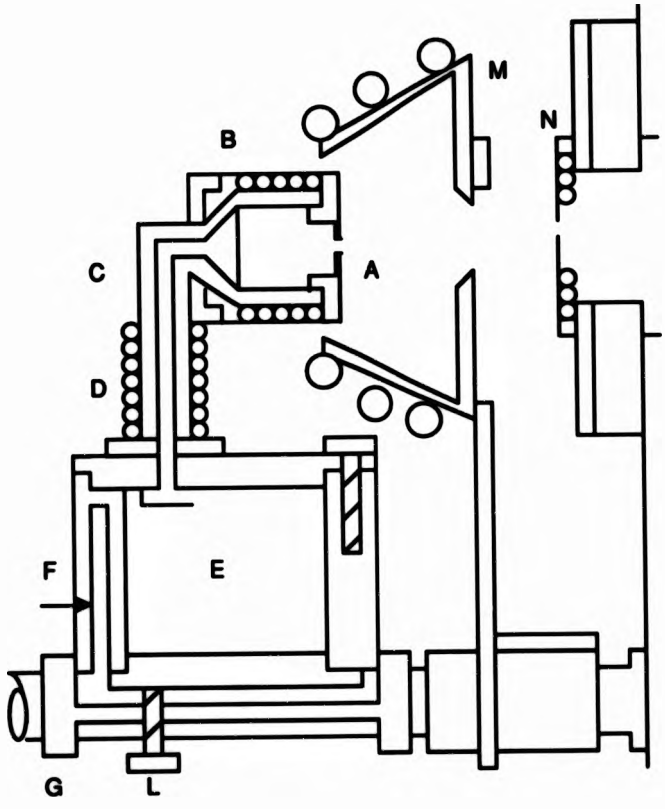

Figure 12: The oven assembly

A difference of 30°- 50° is always maintained between the nozzle and the main body. The operating temperature for sodium is 350°C for the main body and 390°C for the nozzle and the operating condition for potassium is 270°C for the main body body and 300°C for the nozzle . This temperature difference prevents any clogging of the nozzle.

To collect the excess alkali metal, a water cooled condenser is placed in front of the nozzle. The front part of the nozzle can be inserted inside the condenser, so that most of the metal can be collected inside the condenser.

3.3.2 Dimer Reduction and Atomic Beam Intensity

As we have already discussed the oven used is a two stage oven. The first stage is called the main body, which contains the alkali metal. The second stage is the nozzle. The two stages are connected via a tube called the interconnecting tube. The nozzle consists of an aperture in a thin wall, through which the alkali metal effuses to the surroundings.

We assume that the laws of the simple effusion from an aperture in a thin wall and from a long channel hold. Then following Ramsey (1969) and Melissa and Moody (1977) if we let the condition of the main body be denoted by the subscript 2, and that of the nozzle by subscript 1 we indicate the value of density and temperature in such regions by the symbols n and T respectively. If A_{can} is the cross sectional area of the canal of the interconnecting tube and A_{ass} is the cross section of the circular output

aperture of the nozzle, and if $I_\uparrow$ and $I_\downarrow$ are the flow up and down the interconnecting tube, and I_0 is the rate of effusion from the output aperture of the nozzle, then.

$$I_0 = (1/4)\ n_1 \underline{v}_1 A_{nzz}$$
$$I_\downarrow = (1/p)\ \tfrac{1}{4} n_1 \underline{v}_1 A_{can}$$
$$I_\uparrow = (1/p)\ \tfrac{1}{4} n_2 \underline{v}_2 A_{can} \qquad \text{(III-1)}$$

The first two equations govern the flow out of the nozzle, and the third governs the flow into the nozzle. The 1/p factor corrects for the fact that the entire connecting tube is not a thin aperture. It is given by

$$1/p = (8/3)\ r/L = 1/8 \qquad \text{(III-2)}$$

where r is the radius of the canal of the interconnecting tube (0.25cm) and L is the length of the interconnecting tube (5.5cm).

The condition which must be met in equilibrium is

$$I_0 = I_\uparrow - I_\downarrow \qquad \text{(III-3)}$$

From (III-1) and (III-3) we get

$$\frac{n_1}{n_2} = \frac{\underline{v}_2}{\underline{v}_1} \frac{1}{[p\ (A_{nzz}/A_{can}) + 1]} \qquad \text{(III-4)}$$

since $\underline{v} = (8kT/\pi M)^{\frac{1}{2}}$

then $\underline{v}_2/\underline{v}_1 = (T_2/T_1)^{\frac{1}{2}}$ (III-5)

where T_2 is the temperature of the main body and T_1 is the temperature of the nozzle.

Since $A_{nzz}/A_{can} = (5/3)^2$

(III-4) becomes

$$n_1/n_2 = (0.446)(T_2/T_1)^{\frac{1}{2}} \qquad \text{(III-6)}$$

The operating temperatures for the main body and the nozzle for sodium atoms are T_2(M.B.) = 623K and T_1(Nzz) = 663K

So, $n_1/n_2 = 0.419$ (III-7)

The corresponding operating temperatures for potassium are

T_2(M.B.) = 538K and T_1(Nzz) = 573K

So, again

$$n_1/n_2 = 0.419 \qquad \text{(III-8)}$$

By running the nozzle at higher temperature than the main body, we find not only that the density of the alkali metal in the nozzle region comes to about half of that in the main body region, but also that we get a reduction in the dimer density (Melissa *et al*, 1977).

To make a quick estimation of the intensity of the atomic beam we follow Ramsey (1969).

Let $N(\theta)d\Omega$ be the number of particles per second effusing into a solid angle at an angle θ with respect to the normal of the area A_{nzz} of the source then

$$N(\theta)d\Omega = \frac{n\bar{v}A_{nzz}}{4\pi}\cos\theta d\Omega \qquad \text{(III-9)}$$

here n is number of particles per unit volume in the enclosure and

$$\underline{v} = \left(\frac{8kT}{\pi m}\right)^{1/2} \qquad \text{(III-10)}$$

is the average velocity of atoms.

For sodium $\underline{v} = 7.812 \times 10^4$ cm/sec

and for potassium $\underline{v} = 5.572 \times 10^4$ cm/sec.

Integration of (III-9) yields the total number of particles per second, N, escaping through the aperture.

$$N = n\underline{v}A_o/4 \qquad \text{(III-11)}$$

where v is the average velocity of the atoms , A_o=0.018 cm^2, is the area of the source (nozzle) and n=p/kT is the density of the atoms in the main body , where p is the vapour pressure inside the main body of the oven and k is Boltzman's constant. For sodium ,

p_{Na} =1x10^{-1} mmHg at 623K(main body), and for potassium

p_K =9x10^{-2} mmHg at 538K(main body) .

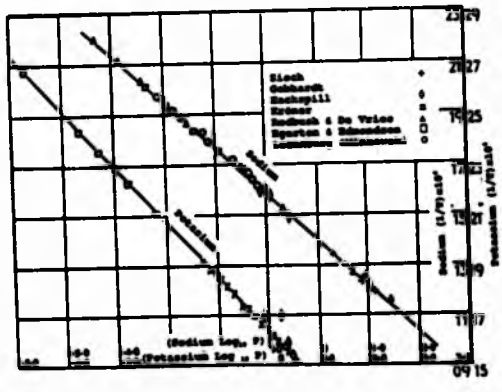

Figure 13. Vapour pressure/temperature relation of sodium and potassium. T is in K and P in mm of Hg

So , for sodium

n_{Na}(main body) $=1.55\times10^{15}$ atoms/cm^3 ,

and for potassium

n_K (main body)$=1.63\times10^{15}$ atoms/cm^3.

The density n_1 in the nozzle is related to the density n_2 in the main body by III-6 . For sodium the density n_{Na} in the nozzle is,

n_{Na}(at the nozzle)$= 0.67\times10^{15}$ atoms /cm^3 ,

and for potassium

n_K(at the nozzle) $= 0.7\times10^{15}$ atoms/cm^3.

Thus the rate of effusion for sodium and potassium is given for sodium by :

$$N = 2.7 \times 10^{17} \text{ atoms/sec} \qquad \text{(III-12)}$$

and for potassium by :

$$N = 1.8 \times 10^{17} \text{ atoms/sec} . \qquad \text{(III-13)}$$

The forward peak intensity which is accepted and transmitted through the hexapole magnet in either spin state is given by Hils (1971) as

$$I_\pm = (N/\pi)\Omega_\pm \qquad \text{(III-14)}$$

where (±) refers to the spin up or down components and ($\Omega_\pm$) is the solid angle of acceptance of the hexapole magnet for the two spin states. An estimate of the solid angle of acceptance for spin up atoms is given in the next section.

3.3.3 The Hexapole Magnet

Friedburg (1951) was the first scientist to introduce the hexapole (sixpole) magnet. This magnet can be used for two purposes; the first one is to separate the magnetic spin states from each other (see Hughes, 1971); and the second is to use its properties to focus one magnetic spin state and defocus the other.

The hexapole magnet is approximately in the shape of a cylinder whose wall potential varies as $\sin(n\theta)$, where θ is the azimuthal angle, and n is a positive integer.

If we have N pairs of pole tips with each tip occupying an angle α on the cylinder of radius r_o and if the potential alternating from one pole to the next as $\pm V$, and if the potential is zero on the axis of the cylinder, then the magnetic potential $\Phi(r,\theta)$

$$\Phi(r,\theta) = \frac{4V}{\pi} \sum_{n=1}^{\infty} \left(\frac{r}{r_o}\right)^n \frac{\sin n\theta}{n} \sin\frac{n\alpha}{2} \sum_{l=1}^{N} (-1)^{l-1} \times \sin\left[\frac{n}{N}\pi(2l-1)\right] \qquad \text{(III-15)}$$

In terms of the magnetic field, and since $\mathbf{H} = -\nabla\Phi$ the above equation leads to,

$$H = H_o \left(\frac{r}{r_o}\right)^2 \left[1-2\left(\frac{r}{r_o}\right)^6 \cos 6\theta + \left(1-2\cos 12\theta\left(\frac{r}{r_o}\right)^{12}\right) + \ldots\right]^{1/2} \qquad \text{(III-16)}$$

where r, is the radial distance from the hexapole axis to the point of study

r_o, is the radius of the hexapole magnet = 0.159 cm

and H_o , is the field of the hexapole magnet at the tip of the pole = 8600 G measured by Tesla meter 904(RFL)

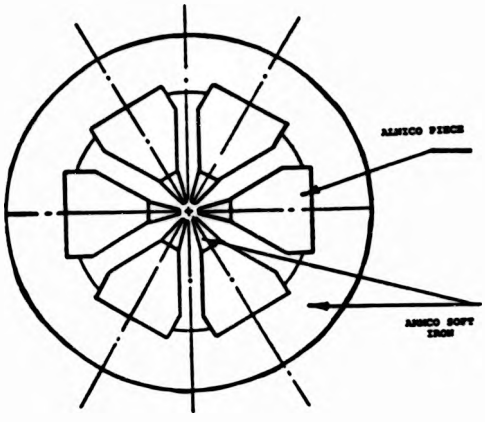

Fig 14. Hexapole permanent magnet. Cylindrical yoke and pole tips are Armco iron; pyramid-shaped poles are Alnico V.

Our hexapole magnet is 7.6 cm long with a radius of r_o = 0.159 cm, and each pole tip occupies an angle $\alpha = 30°$. If we have N = 3 pairs then

$$H = H_o \left(\frac{r}{r_o}\right)^2 \qquad \text{(III-17)}$$

The energy, E, of an atom with magnetic moment μ in a magnetic field H, is given by

$$E = -\mu.H, \qquad \text{(III-18)}$$

so, whenever μ is constant and parallel to an associated angular momentum and any variation in H is applied slowly

(ie, in many cycles of Larmor precession of the moment in the field), then the projection of μ on H remains constant (ie, there is no change of quantum state). We notice also that the direction of H has no effect on the energy of the system. The field inside the hexapole magnet varies from a weak field due to penetration of the earth magnetic field at the axis of the Hexapole magnet, to a strong magnetic field at the tips of the hexapole. The forces acting on the atom inside the hexapole are

$$F = -\nabla_r E = -(\delta E/\delta H)\nabla|H| \qquad \text{(III-19)}$$

writing $\delta E/\delta H = -\mu_{eff}$ from III-18, (III-20)

$$F = 2\mu_{eff} H_o (r/r^2_o) \qquad \text{(III-21)}$$

The behaviour of the effective magnetic moments of the atom, of nuclear spin I=3/2 , with the magnetic field is shown in figure 15 taken from Ramsey (1969)

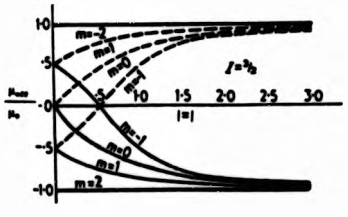

Figure 15. Variation of the effective magnet moment with the magnetic field. The dotted lines are the moments of the magnetic levels arising from the F = I−½ state. The nuclear moment is assumed positive.
$x = -\dfrac{(\mu_o/J)H}{\Delta E}$.

By studying carefully the graph above, we conclude that at higher magnetic field

$$\mu_{eff} = -m_J g_J \mu_o \quad \text{(Christensen, 1959)} \qquad \text{(III-22)}$$

$$= \pm \mu_o$$

where μ_o = Bohr magneton

so,

$$F_+ = - \frac{2\mu_o H_o}{r^2_o} r \qquad \text{(III-23)}$$

and,

$$F_- = + \frac{2\mu_o H_o}{r^2_o} r \qquad \text{(III-24)}$$

Thus atoms with $\delta E/\delta H > 0$ and thus $m_J > 0$, (equation III-23) find themselves acted upon by a force directed always towards the hexapole axis. In this case the motion transverse to the axis is a simple harmonic motion. These atoms are focused and used for the experiment. Atoms with $\delta E/\delta H < 0$ and thus $m_J<0$ (equation III-24), find themselves repelled away from the hexapole axis in a hyperbolic path, ie these atoms are defocused out of the beam and can not be used in the experiment. By drawing the Breit-Rabi diagram for a spin ½ particle with nuclear spin 3/2, we can make this even more apparent as shown in figure (16) taken from Ramsey (1969).

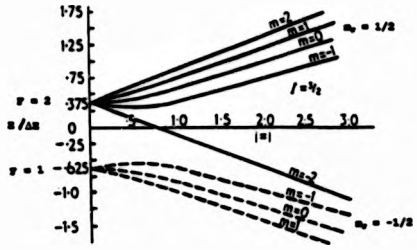

Figure 16. Variation of the energy with the magnetic field. Nuclear moment assumed positive, $J = \frac{1}{2}$. The dotted lines are the magnetic levels arising from the $F = I - \frac{1}{2}$ state. The level structure corresponds to the ground state of sodium and potassium. ΔE is the energy difference between F=2 and F=1 at zero magnetic field.

In figure 17 we show what happens to the atoms.

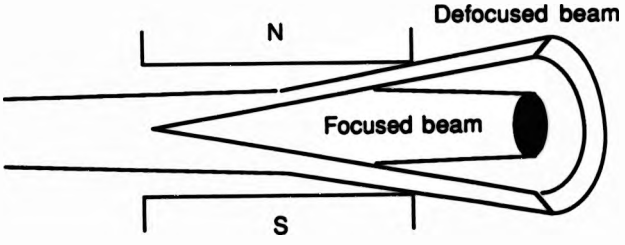

Figure 17. The focused and the defocused component of the atomic beam after passing through a short hexapole magnet.

The atoms which enter the hexapole at an angle with the hexapole axis, will be acted upon by a force and they will suffer a deflection according to equations (III-23) and (III-24). In the case that an atomic beam effuses from the aperture of a nozzle, the hexapole entrance will subtend a solid angle, Ω, at the nozzle aperture which is located at a distance, L_1, away from the entrance of the hexapole. If the initial velocity of the atoms is v and at a small angle ϕ_0 to the axis, then at distance x, measured within the magnet, the equation of the trajectories for the atoms with

magnetic quantum number $m_z > 0$ is given by Christensen (1959) by the fomula ,

$$r(x) = \phi_0 [L_1 \cos(\omega x/v) + (v/\omega) \sin(\omega x/v)] \qquad \text{(III-25)}$$

where x is the distance measured within the magnet and for atoms with magnetic quantum number $m_z < 0$

$$r(x) = \phi_0 [L_1 \cosh(\omega x/v) + (v/\omega) \sinh(\omega x/v)] \qquad \text{(III-26)}$$

where $\omega = \dfrac{(2\mu_{eff}H_0)^2}{mr_0^2}$, for a $^2S_{\frac{1}{2}}$ state and large H_0

$$\omega = \frac{(2\mu_0 H_0)^2}{mr_0^2} \qquad \text{(III-27)}$$

where μ_0 = the Bohr magneton

and L_1 = 11cm, the distance from the beam source to the hexapole entrance. The acceptance solid angle of the hexapole for spin up atoms is given by

$$\frac{\Omega+}{4\pi} = \phi^2_0/4 = \frac{1}{4} \cdot \frac{r_0^2}{L_1^2 + (v/\omega)^2} \qquad \text{(III-28)}$$

and that for spin down atoms by

$$\frac{\Omega-}{4\pi} = \frac{1}{4} \cdot \frac{r_0^2}{[L_1 \cosh(\omega L_2/v) + (v/\omega)\sinh(\omega L_2/v)]^2} \qquad \text{(III-29)}$$

where L_2 = 7.6cm is the hexapole magnet length. To estimate the intensity of the spin up atoms, we have to calculate $\Omega+$ using (III-28)

$$\Omega+ = \frac{\pi r_0^2}{L_1^2 + (v/\omega)^2} \qquad \text{(III-30)}$$

We notice that all quantities, especially r(x) and Ω_+ depend

on the velocity of the atoms. One therefore has to average over the velocity distribution in the atomic beam. So,

$$< \Omega_+ >_v = \frac{\int_0^\infty f(v)\ \Omega_+\ dv}{\int_0^\infty f(v)\ dv} \qquad \text{(III-31)}$$

where, $f(v) = (2I_o/\alpha^4)\ v^3 \exp(-v^2/\alpha^2)$ (Ramsey, 1969)

$\alpha = (2kT/m)^{1/2}$, is the most probable velocity

$I_o = \int_0^\infty f(v)\ dv$ is the total intensity.

With the help of an existing computer program package (MATHCAD, Math Soft Inc) the average solid angle of acceptance for spin up atoms of the hexapole magnets has been calculated: For sodium, at temperature 663K,

$$< \Omega_+ >_v = 4.234 \times 10^{-4} \text{ st} \qquad \text{(III-32)}$$

and for potassium, at temperature 573K,

$$< \Omega_+ >_v = 4.9 \times 10^{-4} \text{ st.} \qquad \text{(III-33)}$$

Since the intensity which is accepted by the hexapole magnet is given by (III-14)

$$I_+ = (N/\pi) < \Omega_+ >_v$$

it follows that the intensity for sodium is

$$I_{+(Na)} = 3.6 \times 10^{13} \text{ atoms/sec} \qquad \text{(III-34)}$$

and for potassium

$$I_{+(K)} = 2.8 \times 10^{13} \text{ atoms/sec.} \qquad \text{(III-36)}$$

3.3.4 Guiding fields and low field polarisation

When we explained the hexapole magnet, we mentioned that, if an atom possesses a magnetic moment μ and if μ is fixed in magnitude and linked to an associated angular momentum, there would be no change of state of the atom if any variation in $\mathbf{H}$ were carried out slowly (ie, in many cycles of the Larmor precession of the magnetic moments in the field). Of course, this condition is met inside the hexapole magnet. But problems can arise when the atoms leave the hexapole magnet and move into the low field region in which the scattering experiments are to be carried out. Especially when the field is close to zero even a small field change can be quite abrupt to the atoms and cause a change of state and thus depolarisation of the atomic beam. To prevent this depolarisation the atomic beam was guided adiabatically, using coils, from the hexapole magnet up to the interaction region and to the Rabi detector when required.

In a strong magnetic field such that occurs inside the hexapole magnet the polarisation of the atomic beam could theoretically be 100%. The actual polarisation of the atomic beam in the strong magnetic field of the hexapole magnet used has been calculated by Hils *et al* (1981) to be P_a=70% .

In the weak field the polarisation is reduced by hyperfine structure coupling of $\mathbf{I}$ and $\mathbf{J}$ to $\mathbf{F}$ to a maximum theoretical value of

$$P_{max} = \frac{1}{(2I + 1)} \times 100 \ \% \qquad \text{(III-36)}$$

where I is the nuclear spin of the atom involved. For sodium and potassium I = 3/2, so, that P_{max} = 25% . The maximum polarisation which has been achieved experimentally for the alkali atom beam is 21% as measured in the present experiment using a combination of Rabi magnet and Langmuir - Taylor detector. Figure 18 shows the profile of the potassium beam obtained in the present study from which we can calculate the polarisation of the potassium beam.

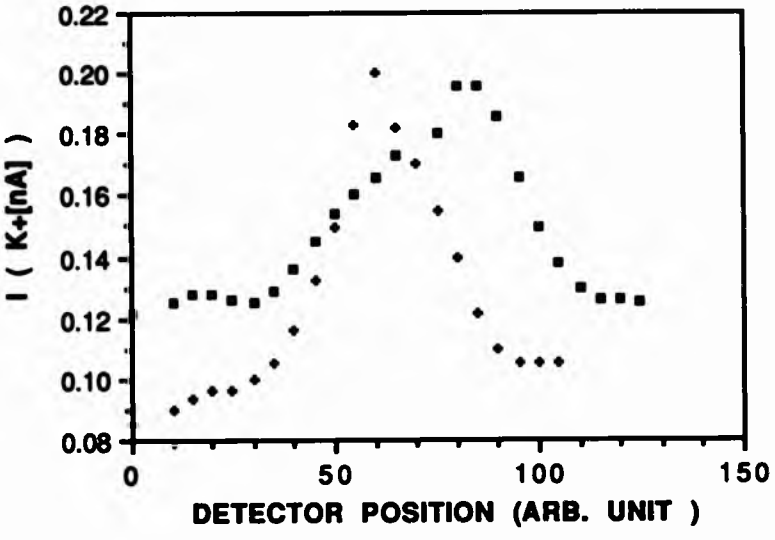

Figure 18. The atomic beam profile of the potassium atom measured by the Langmuir-Taylor detector (50 =0.115 cm).
(a) ♦ refers to the undeflected beam (Rabi magnet off)
(b) ■ refers to the deflected beam (Rabi magnet on).

3.3.5 The Rabi Magnet

The Rabi magnet provides an inhomogeneous magnetic field of a pattern which allows the spin analysis of atomic beams. It is made of soft iron which is magnetized by coils when required. The idea of this magnet was first proposed by Millman, Rabi and Zacharias as quoted by Ramsey (1969) and shown in Figure 19.

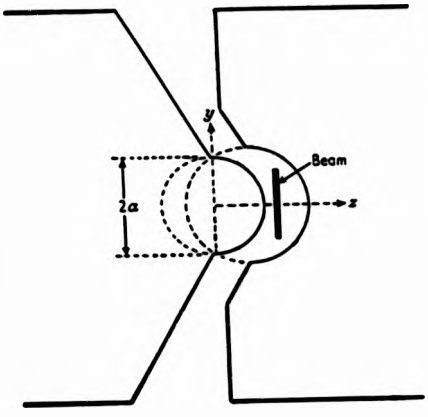

Figure 19. Typical cross-section of the pole pieces of a Rabi magnet effectively producing two-wire fields. The direction of the beam is perpendicular to the plane of the paper ,Ramsey(1969)

This kind of design has the advantage that its boundaries correspond to the equipotentials of the field produced by a system of the two parallel wires system(Ramsey, 1969).

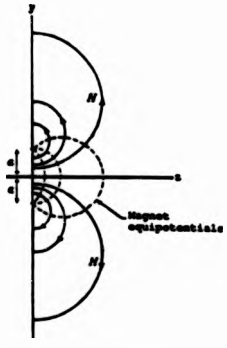

Figure 20. Magnetic field around two-wire field (full curves) and magnetic equipotentials (dashed curves). Infinitely narrow wires are assumed in the figure but outside the wires the field is independent of the wire diameter

This design gives a uniform magnetic field gradient over the beam height situated as shown in fig 19. The height of the slit is 8mm and its width is 0.1 mm. According to Goudsmidt and Uhlenbeck a permanent magnetic moment is assigned to the electron which derives from an intrinsic angular momentum (spin) determined by a fixed quantum number s = ½. In the case of ground state sodium or potassium passing through the Rabi magnet, the atoms will suffer a deflecting force given by

$$F = \mu_z \, (dH/dz) \qquad \text{(III-37)}$$

where $\mu_z = g_J \, m_J \, \mu_B$, in a strong magnetic field.

For Na and K

$m_J = \pm ½$ and $g_L = 2$ for K and Na

$\mu_z = \pm \mu_B$

and $F = \pm \mu_B (dH/dz)$ (III-38)

When the Rabi magnet is on, the beam profile splits into 2 more or less well resolved traces which allows the polarisation of the atomic beam to be deduced , see fig (18). The polarisation of the beam is given by

$$P = \frac{N_1 - N_2}{N_1 + N_2} \qquad \text{(III-39)}$$

where

N_1 = number of atoms with spin up

N_2 = number of atoms with spin down

3.3.6 Langmuir-Taylor Detector and Atomic Beam Density

The Langmuir-Taylor detector is a surface ionization detector , see fig (21). Our detector is made of a 3cm long tungsten wire of 0.1mm diameter with a copper cylinder surrounding it. This wire is placed on the axis of a copper cylinder and held taut by two screws. The tungsten wire was oxidised by flashing it in air for a second (black coated). A 1cm hole in the surface of the cylinder lets the atomic beam pass through. The detector was placed inside another cylinder and isolated from it by ceramic spacers. The outer cylinder was attached to a vertical drive held by a bellow so that the detector can be moved up and down.

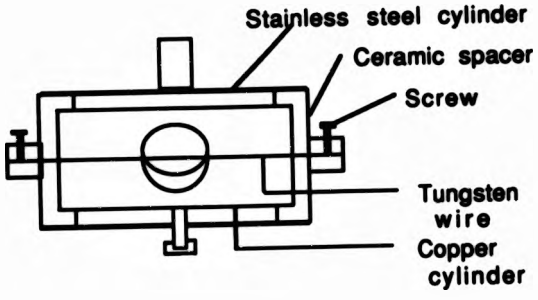

Figure 21: Langmuir-Taylor detector

The idea of this detector is to ionize the atoms which strike the wire, and to collect the ions by the copper cylinder. For this purpose a current of 0.84A was passed through the wire which is biased positively with respect to the copper cylinder. If I is the ionization potential in eV, T the temperature of the wire and Ø the work function of the wire in eV, we have

$$n^+/n = \exp(\phi - I)/kT \qquad \text{(III-40)}$$

where n^+/n is the ratio of the re-evaporated ions n^+ to the number of the re-evaporated neutral atoms n, and k the Boltzman constant $k = 8.5 \times 10^{-4}$ eV/K .

Every atom which strikes the wire will be ionised when the following condition is fulfilled.

$$(\phi - I) \geq 0.5 \text{ eV} \qquad \text{(III-41)}$$

Thorium-free tungsten has a work function of 4.48 eV which can be increased by surface-oxidisation to 6eV. Thus the detector works at its best condition for both sodium and

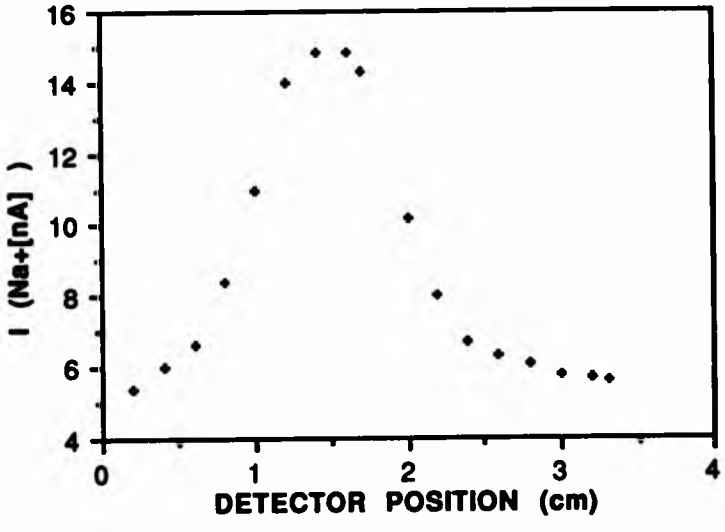

Fig. 22 Sodium beam profile

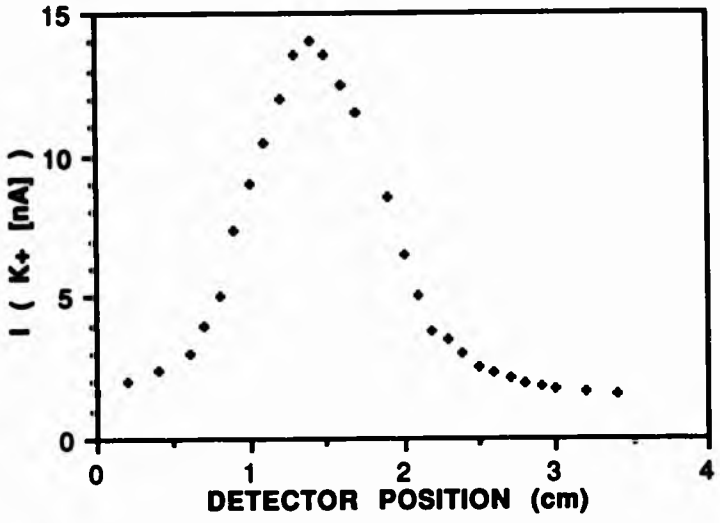

Fig. 23 Potassium beam profile

potassium without the need to change the wire (I_K = 4.1 eV, and I_{Na} = 5.13 eV). The profile of the detected potassium atomic beam, 112.5cm away from the hexapole magnet is shown in figure (23) and the atomic beam density at the magnet end (n_{ex}) is related to the density at the detector (n_{det}) by

$$\frac{n_{ex}}{n_{det}} = \left(\frac{D_{det}}{D_{ex}}\right)^2 \qquad \text{(III-42)}$$

where D_{det} and D_{ex} are, respectively, the beam diameters at detector and at the hexapole exit. (D_{ex} = 0.2cm, Hils, 1971)

Also $$n_{det} = \frac{i_{ion}}{l_w . D_w . \underline{v} . e} \qquad \text{(III-43)}$$

where i_{ion} is the ion current,

l_w = 1cm is the length of the wire exposed to the atomic

beam, D_w = 0.1mm is the wire diameter,

$\underline{v} = \left(\frac{8kT}{\pi m}\right)^{\frac{1}{2}}$ the average atomic velocity,

and e the electronic charge . For sodium,

$\underline{v}$ = 7.812 x 10^4cm/sec (T=660K)

and for potassium,

$\underline{v}$ = 5.572 x 10^4cm/sec. (T=573K)

Then for sodium ,

n_{det} = 1 x 10^{+14} atoms/m^3 (III-44)

and for potasium

n_{det} = 1.5 x 10^{+14} atoms/m^3 (III-45)

Substituting III-44 and III-45 into III-42 we get n_{ex}.

For sodium

$n_{ex(Na)}$ = 2.50 x 10^{+15} atoms/m^3 (III-46)

and for potasium we get

$n_{ex(K)}$ = 3.8 x 10^{+15} atoms/m^3 (III-47)

The beam diameter ($D_{I.R}$) at the interaction region which is 38.5cm away from the hexapole magnet axis is

$D_{I.R}$ = 0.41cm

so, that the density of the atomic beam at the interaction region can be given by;

$$n_{I.R} = n_{det}\left(\frac{D_{det}}{D_{I,R}}\right)^2$$

For sodium

$n_{I.R}$ = 6.0 x 10^{+14} atoms/m^3 (III-48)

and for potassium

$n_{I.R}$ = 9.0 x 10^{14} atom/m^3 (III-49)

3.4 THE ELECTRON BEAM COMPONENTS

3.4.1 Electron Gun

The basic problem in designing an electron gun is to produce the maximum current required, and if all other parameters are fixed, then this will place stringent limits on the maximum attainable current. To build a low energy, high current electron gun, Simpson and Kuyatt (1963) used a multistage design. This idea is based on the observation in unipotential guns such as diodes, that, below a certain minimum voltage,the electron beams of these guns cannot saturate a given space. So if an electron beam of energy E passes through a region of length (l) defined by two apertures of diameter $2r_o$ and if the maximum convergence angle of these apertures is γ then there are two restrictions on the maximum current which can be put through.

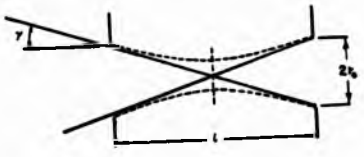

Figure 24. Dotted line shows idealized space charge-limited beam profile required to saturate a given space

The first restriction is due to the repulsive force between electrons when they come very close to each other, i.e. the space charge force which is independent of l and r_o but depends on the ratio l/r_o.

Provided that any external magnetic field is compensated and

that the electron beam enters the space with a maximum angular spread 2γ such that the extreme rays would cross in the middle of the space as shown in Figure 24 then the maximum current which can be put through that region is

$$I_{max} = 38.5E^{3/2} (2r_o/l)^2 = 38.5E^{3/2} \tan^2\gamma$$

where I_{max} is in μA and E in eV . The electrons move in the middle of the space parallel to the axis of the apertures and the electron beam forms a disc of diameter $2r_o/2.35$.

The second restriction on the electron beam is imposed by the theorem of Helmholtz - Lagrange which states, that for any two planes Z_1 and Z_2 seperated by a non-absorbing optical path, such that plane Z_2 is the image of plane Z_1,

$$n_1 dx_1 \sin\theta_1 = n_2 dx_2 \sin\theta_2$$

Here n_1 and n_2 are indices of refraction, θ_1 and θ_2 are angles of convergence at points in plane Z_1 and Z_2, and dx_1 and dx_2 are differential elements in the planes (Simpson, 1967). According to this theorem Simpson and Kuyatt dealt with limitations on beam density of unipotential guns. They obtained the following expression which relates the cathode temperature T (in K), the electron convergence angle at the anode, θ_2, and the angle γ , characterising the dimension of the gun to the electron energy E

$$E \geq \left(\frac{211}{\pi}\right) \left(\frac{T}{11600}\right) \left(\frac{\tan^2\gamma}{f(\gamma)\sin^2(\theta_2)}\right) \qquad \text{(III-50)}$$

This inequality must be satisfied for saturation of the space.

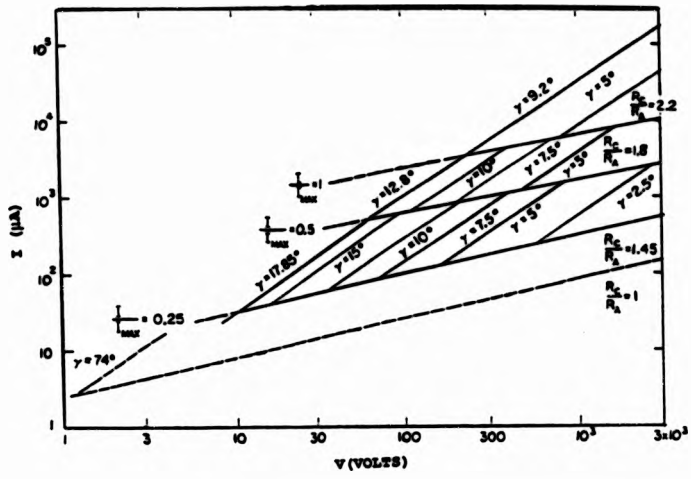

Figure 25 Graph of current vs. voltage showing regions accessible to diode guns capable of obtaining space charge saturation current, I_{max}, within a given space defined by convergence angle . Cases of less than full saturation $0.5I_{max}$ and $0.25I_{max}$ are also shown. The usable region is to the right of the γ = constant and above the I/I_{max} = constant lines. On the right margin is given the cathode to anode radius R_c/R_a of the optimum Pierce gun. The dashed line at the bottom is the zero anode-cathode spacing limit, see Simpson and Kuyatt (1963).

In figure (25), taken from Simpson (1967), the line I/I_{max} = 1 represents the condition given by the equality of equation (III-50), while other lines which are parallel to this line represent currents less than I_{max}. Also shown are lines of equal perveance $I/V^{3/2}$, as straight lines sloping upwards to the right. The way to use this graph is to use the regions to the right of γ = constant and above the appropriate current ratio line. We see that no space can be saturated with a unipotential gun of less than 220 V anode voltage for

the region determined by the line $I = I_{max}$ and $\gamma = 9.2°$ and that for 10 volts the most that can be expected from such a gun is 25% saturation with a convergence angle of 17.85°, at a current of about 20μA. At 1 volt the convergence angle γ would be greater than 74°, and these highly divergent diodes are unsuitable for the present experiment. It is also found for a triode gun with a hairpin filament that its plane of smallest electron beam cross section occurs within the gun and the beam diverges from then on as seen in figure (26)

Figure 26. The formation of the smallest cross section within the gun.

The multistage construction of the gun essentially overcomes these difficulties by extracting the electrons at some higher energy to overcome the space charge problem and by then decelerating the electron beam to its final energy. In our case where the cathode is biased negatively, the image of this cathode forms the plane of the smallest cross section. This image is transferred through the various parts of the gun until it forms a reduced image at the interaction region. The contour of the electron beam at the interaction region will be similar to Figure (24)

The electron gun design is shown in figure (27). The first stage of this gun consists of the cathode(0), grid(1) and anode(2) ,all are made of tantalum. This extraction stage

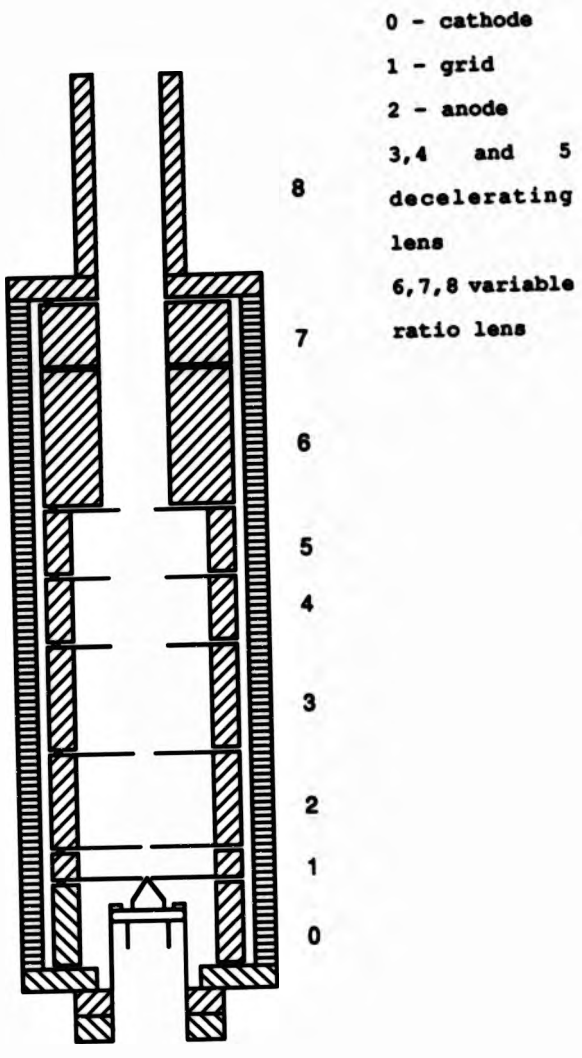

Figure 27: cross section of the electron gun to scale

forms a Soa - type immersion lens, which has the property that the object and the image lie within the lens field. So, the lens will form an image of the cathode at some intermediate position which is a function of $\gamma = V_g / V_a$ as

given by Soa (1959) as quoted by Simpson and Kuyatt (1963). The magnification and position of the cathode image is greatly influenced by the grid bias. So, by increasing the biasing of the grid the image of the cathode will move further and further away from the anode.

At zero or small negative bias the reduced image of the cathode will appear in close vicinity to the anode plane as shown in graph (28).

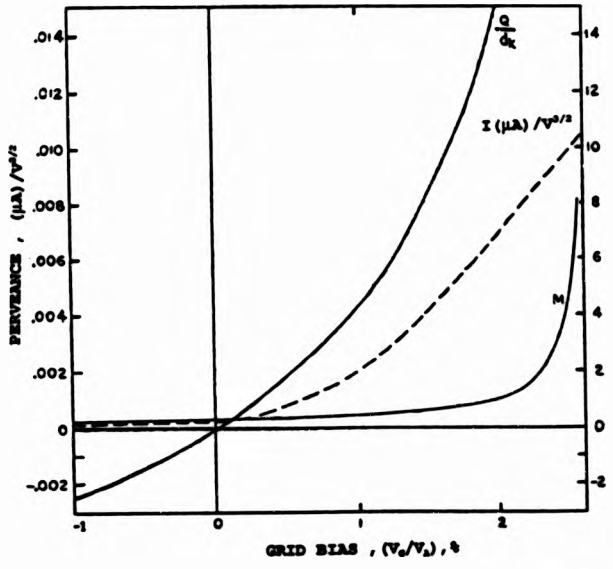

Figure 28. Properties of a standard Soa immersion lens. The scale invariant parameter perveance, $I/V^{3/2}$, is given on the left ordinate, the optical properties, image distance Q in units of grid cathode spacing d_k and magnification M on the right. The distance Q is measured from the anode plane. The values of grid bias are relative to the cathode surface. The effect of contact potential, interface drop, etc. may be as much as 2V. The zero bias point was determined by the break in curves of current vs applied bias.

The second stage which is a deceleration stage consists of three aperture lenses 3, 4, and 5 which allows the demagnified image to be projected onto a reduced image in the interaction region. These two stages together can be used as a low energy gun, but in our work we tried to avoid any unwanted electric and magnetic fields. So, a third stage was added to overcome this problem by using a variable ratio lens, again machined out of non-magnetic stainless steel, such that the last element towards the interaction region is earthed while the entrance is held at the same potential as the exit aperture of the deceleration stage. In these circumstances the cathode should be biased negatively and the energy of the electrons is given by the absolute value of the cathode bias after taking into account the contact potential.

3.4.2 The contact potential

As we mentioned before, our cathode is a hairpin tungsten wire heated directly by the passsage of electric current. The various other parts of the electron gun are made of different materials, tantalum and non-magnetic stainless steel. All these materials have different work functions relative to the vacuum and will produce a net contact potential. To reduce this contact potential , V_c, all the metal surfaces which surround the interaction region and the aluminium table which holds the lens holder are coated with aquadag. The potential difference between the interaction region and the cathode does not give the real energy of the electrons because of the existence of these "contact potentials".

Subsidiary measurements were done to derive the value of the contact potential for each data set (sodium and potassium). For the case of potassium a photomultiplier in combination with an interference filter was used to detect the radiation of the potassium line (404.4nm) ($5P_{3/2} - 4S_{\frac{1}{2}}$). The cathode potential with respect to earth was changed in steps of 1V near threshold for the excitation process and photons were observed at each potential step. A graph of the photon counts as a function of the cathode potential, is shown in figure 29.The potential corresponding to the intersection of

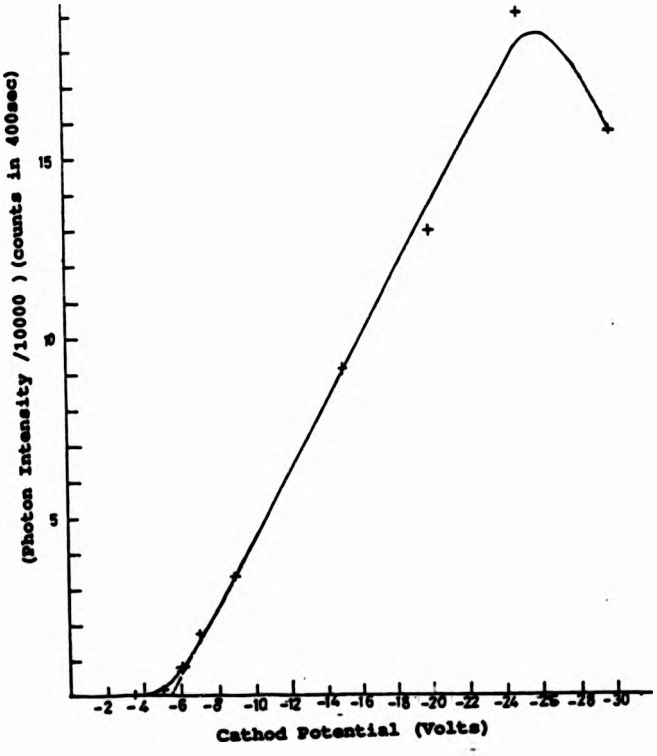

Fig (29) Determination of the contact potential

the straight part of the curve with the zero intensity axis should be the excitation potential of the $5P_{3/2}$ level known to be 3.06V. The difference between this value and that observed corresponds to the contact potential. In the case of the measurement illustrated in figure (29), the measured potential for the excitation of the $5P_{3/2}$ states is found to be 5.5V so that the contact potential is 2.44eV. Thus, for a nominal energy 10eV, for instance, the true energy would be 7.56eV.

3.4.3 The Faraday Cup

The Faraday cup is made of non-magnetic stainless steel, in the form of a cylinder of diameter 0.8cm and depth 6.8cm, the wall thickness being 1mm. The Faraday cup is enclosed in another cylinder of diameter 1cm and depth 7.3cm. A teflon spacer was used to insulate the Faraday cup from the enclosure which is earthed to avoid any stray elecric field at the interaction region. The Faraday cup itself is connected to an electrometer (Keithley, Model 610 CR) to measure the electron current. The Faraday cup, as we notice, is deep; the ratio of its depth to its diameter is about 7, and this ratio provides greater efficiency in collecting the electrons. The efficiency has been improved by sooting the inside of the Faraday cup to prevent electrons from being reflected.

3.4.4 Aquadag and sooting

Various parts of the apparatus are either sooted or aquadagged. This blackening was done for two purposes: the

first purpose was to reduce the photon background and the second was to reduce electron reflection at the metal surface.

Since we used a hairpin filament which produces intense radiation in the visible region it is wise to soot the elements of the electron gun too, to reduce the photon background. This also reduces electron reflection. All parts surrounding the interaction region were aquadagged for the same purpose. The reflection of electrons from an aquadagged surface is five times larger than from a sooted surfaces, see Martin and Engel (1977). So, sooting the electron gun elements will help in producing a better quality electron beam.

3.5 PHOTON DETECTION SYSTEM

3.5.1 Small Helmholtz Coil (Quantization field)

The aim of the experiment is to be able to detect all the relevant polarisation properties of the light . We choose to perform this experiment such that the spin direction of the atoms is perpendicular to the electron impact axis. The induced fluorescence light is then detected in the direction

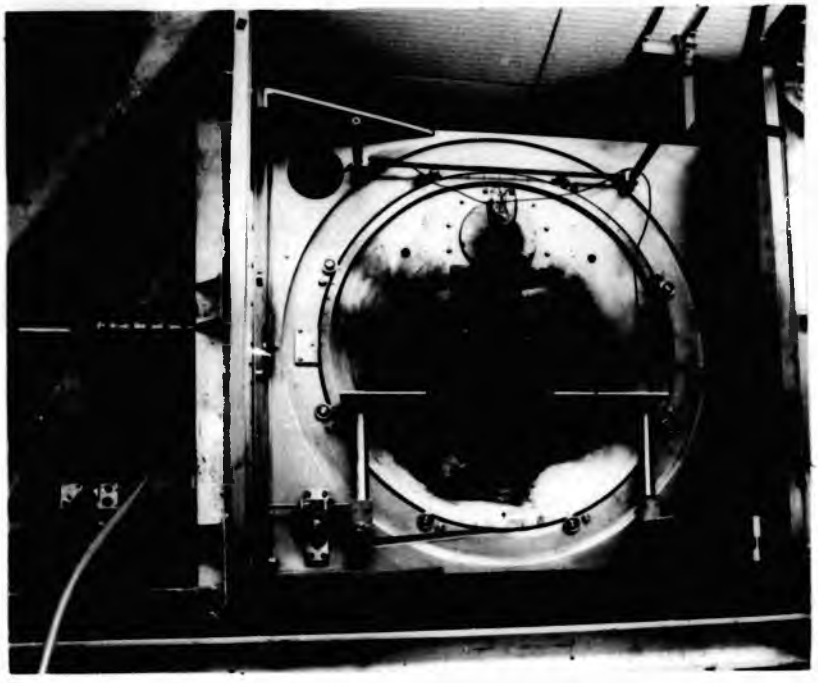

Plate 3: The arrangement of the apparatus at the interaction region.

of the spin polarisation. A small Helmholtz coil pair, each coil with 20 turns, was constructed with a diameter of 3cm and the coils were separated by 1.5cm. These coils not only control the strength of the field in the interaction region but also the direction of the field, which allows the direction of the spin polarisation to be reversed by reversing the field of the Helmholtz coils. Actually, the direction of the spin polarisation is perpendicular to both electron beam and atomic beam at the interaction region. A Thurlby power supply PL370 was used to provide the coil with the required stablised constant current.

3.5.2 Photon detection

The whole system originally was built to do elastic scattering experiments so that no photons were to be detected. In our experiment we are interested in the photons and ignore the scattered electrons. So, we are averaging our result over all electron directions. Some modification had to be done inside the scattering chamber, see plate 3. This modification consists of an aluminium plate held firmly in position by two rods coming off the turntable. This aluminium table holds the small Helmholtz coil described above and the newly designed lens holder whose distance from the center of the interaction region can be adjusted. A plane convex glass lens (Melles Griot) with a focal length of 75mm and an effective aperture of 60mm was used to collect the radiation from the interaction region. The lens was positioned such that it gave a magnified image of the interaction region at the photomultiplier located 63cm away outside the scattering chamber. The vacuum seal was achieved by means of a glass window of 3mm thickness and 40mm aperture. For linear polarisation measurements the light, which was gathered by the lens passed through the glass window and the linear polariser (HN-38) which was fixed in front of the interference filter for the line of interest and then fell on the photomultiplier cathode. The polariser, the interference filter and the photomultiplier all form a single unit which can be rotated manually. For circular polarisation measurements a $\lambda/4$ plate for the line of interest was inserted in the path of the light just outside the scattering chamber and in front of the linear polariser such that its fast axis was set parallel to the

electron beam. A Soleil-Babinet compensator (Halle Nachf) was used to identify and mark the fast and slow axes of the $\lambda/4$ plates. Actually, we used two different photomultipliers in our experiment. A red-sensitive multiplier, specially selected for low dark count rate (EMI, model D-624), was used to measure the Na-D-line (588.9/9.5nm). This 10 dynode tube has fairly small pulses of a few millivolts at an anode voltage of 1600V, and the quantum efficiency at 580nm is 11.8%. The interference filter and $\lambda/4$ plate were those used for the helium yellow line (λ = 588nm). For the blue potassium line (λ = 404.4nm) we used an EMI photomultiplier (model 9883QA). The interference filter (Andover Corporation) for the KI 404.4/404.7nm lines has a peak transmission of 51.5% at 405nm and a bandwidth of 9.7nm. The $\lambda/4$ plate for the line 404.4nm has an aperture of 40mm and is made of mica sandwiched between two glass plates (Dr Steeg & Reuter, type B). Finally we used a linear polariser of the type HN-PB for the potassium line.

3.5.3 The Counting Electronics

A schematic diagram of the counting electronics and of the experimental setup used to measure the Stokes parameters is shown in figure 30. The photomultiplier was powered by a filtered Fluke high voltage power supply, model 408 B. We biased the anode of the photomultiplier positively and the cathode was earthed; at the first stage, ie, between cathode and the first dynode, the electrons are affected greatly by the presence of any magnetic field and this can lead to a loss of signal. To over-come this problem, the

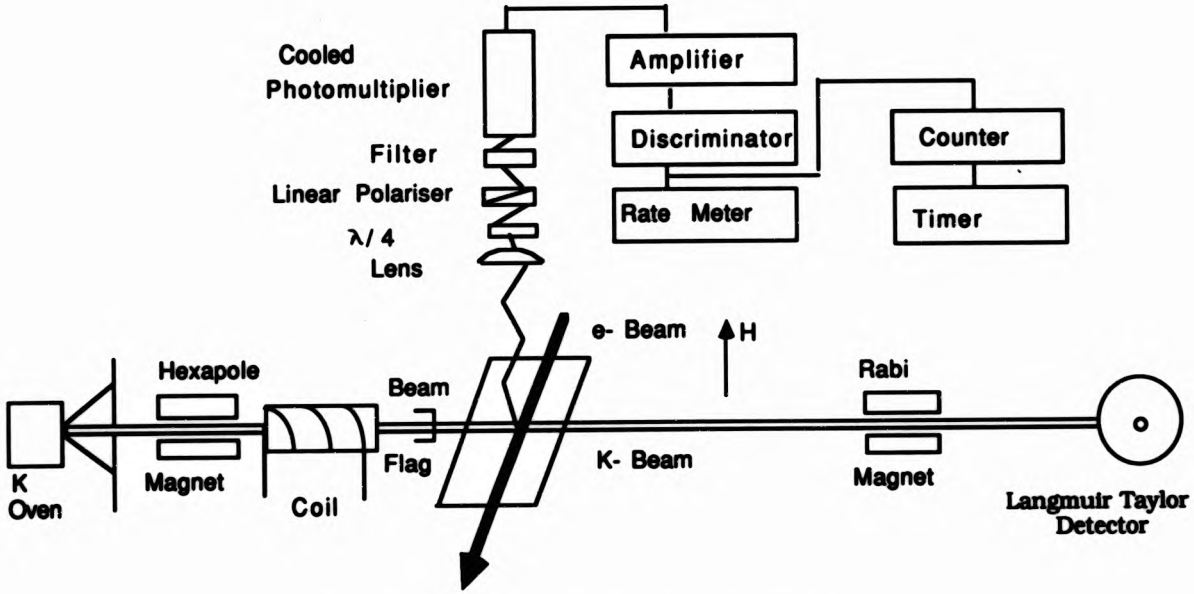

Fig. 30 . Schematic setting of the experiment

photomultiplier was shielded magnetically by soft material (Conetic). The output pulses from the anode were fed to the amplifier (LeCroy, model 612A) which provided amplification by a factor of 10 or a factor of 100, depending on the nature of the signal and the sensitivity of the discriminator. A constant fraction discriminator (Ortec, model 473) was used to cut off the noise from the signal . The signal was then passed to a ratemeter (NE, model 4607), and a linked scaler/timer combination (Nuclear Enterprises) which simultaneously recorded the elapsed time and the number of photons. Preselected time intervals were used during which the number of pulses were counted.

CHAPTER IV

4. THE EXPERIMENT

4.1 Polarisation Measurement and Analysis

4.1.1 Polarisation of the Fluorescence Light

The fluorescent light emitted in the decay of the atom excited by electron impact was detected in the Z-direction. The atomic beam was polarised and its spin polarisation at the moment of impact was also pointing in the Z-direction. The electron-beam, the atomic beam and photon beam form a mutually perpendicular set of cartesian axes. In such an arrangement all the relevant polarisation parameters can be measured using the formulae given by Born and Wolf (1970). In figure 31 we show a generalized arrangement, containing a retarder of retardance Δ and a linear polariser, for the measurement of the polarisation parameters. α is the angle of the polariser transmission axis with respect to the -y-axis (electron beam), and β is the angle of the fast axis of the $\lambda/4$ retarder with respect to the -y-axis. The intensity of the fluorescence light is given in terms of the intensity $I(\alpha, \beta)$ of the light passing through while the transmission axis of the polariser and the fast axis of the retarder are at angles α and β respectively. Hence the intensities are,

$$
\begin{aligned}
I_1 &= I(0°, 0°) + I(90°, 90°) && \text{a} \\
I_2 &= I(45°, 45°) + I(135°, 135°) && \text{b} \qquad \text{(IV-1)} \\
I_3 &= I(45°, 0°) + I(135°, 0°) && \text{c}
\end{aligned}
$$

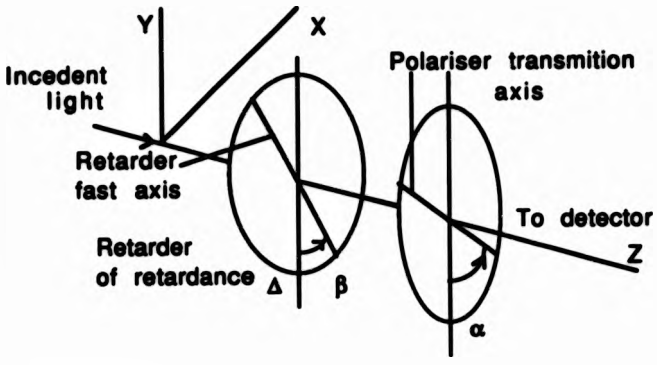

Fig (31) Generalized arrangement of a retarder of retardance Δ and a polariser for the measurement of polarisation parameters.

and, the linear polarisation Stokes parameter P_1 is given by

$$P_1 = \frac{I(0°, 0°) - I(90°, 90°)}{I_1} \qquad \text{(IV-2)}$$

The linear polarisation parameter P_2 is given by

$$P_2 = \frac{I(45°, 45°) - I(135°, 135°)}{I_2} \qquad \text{(IV-3)}$$

and the circular polarisation parameter P_3 is given by

$$P_3 = \frac{I(45°, 0°) - I(135°, 0°)}{I_3} \qquad \text{(IV-4)}$$

Actually in doing the experiment, we used to remove $\lambda/4$ when measuring P_2 .

4.1.2 Correction of the Measured Polarisation

4.1.2.1 Optical Solid Angle Correction

The fluorescence radiation is detected along the OZ axis. As one can see from figure 32 photons which are travelling at a non- zero angle with respect to the Z-axis will be

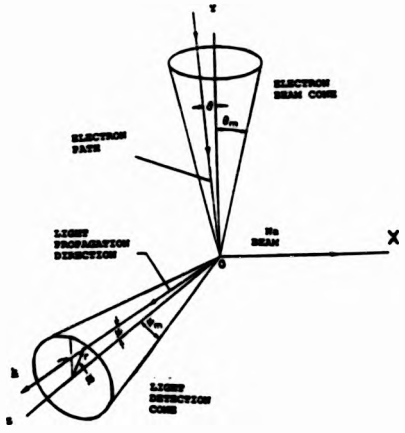

Fig 32 The cordinate system used in calculating the polarisation parameter.

focussed due to the focusing effect of the collecting lens, This will cause a depolarisation of the detected light. A complete derivation for the solid angle correction can be found in Ehlers and Gallagher (1973). We merely report here the formula for this correction. If, as indicated in fig. 32, the atomic beam moves along the x-axis, the electron beam along the - y-axis and ψ_m = 0.33 rad is the maximum acceptance angle for the photons, which is defined by the size of the lens used to gather the light, then the source

polarisation P_s is linked to the observed polarisation P_s' by the equation

$$P_{s'} = \frac{(1-\epsilon)P_s}{(1-\epsilon P_s)} \qquad \text{(IV-5)}$$

where $\epsilon = (1/4)\psi^2_m = 0.027$

The appropriate correction has beenapplied to the measured data.

4.1.2.2 Electron beam divergence

As one can see from figure 32 not all the electrons collide with the atomic beam at right angles. If there is a divergence of the electron beam it will cause the source polarisation, P_s, to be less than the measured polarisation of the photons induced in the excitation process. As we know that the interaction region is 7.7cm away from the second element of the variable ratio lens, which has 1.35cm diameter, so

$$\theta_m = 0.0874 \text{ rad.}$$

where θ_m is the maximum acceptance angle of the electrons. If we define $\delta = (1/4)\theta^2_m = 0.002$ then the source polarisation is given by Ehlers and Gallagher (1973) as

$$P_s = \frac{(1-3\delta)P}{1-\delta P} \qquad \text{(IV-6)}$$

where P is the true polarisation of the electron-excited atoms .And the appropriate correction has been applied to the measured data ,but is found to be small.

4.1.2.3 Analyser transmittance

The polarisation analyser is a polaroid film. This kind of analyser, if not chosen carefully, causes a reduction in the measured polarisation of the detected light due to incomplete extinction of the light if the polariser axis is at a position perpendicular to the E-vector of the detected light. Again, following from Ehlers *et al* (1973), the measured polarisation, P_m , and the polarisation observed through the optics, $P_{m'}$, are related by

$$P_m = \frac{k_\parallel - k_\perp}{k_\parallel + k_\perp} P_{m'} \qquad \text{(IV-7)}$$

where $k_\parallel$ and $k_\perp$ are the transmittances for radiation with the electric vector parallel or perpendicular to the polariser axis.

In our experiment, we applied two different analysers. For the sodium D-line (589 nm), we used HN-38 polaroid film which has a transmission of 38% and for the potassium line (404.4 nm) we used NH-PB film, which has a transmission of 30% at this wavelength. Both analysers provide a high extinction ratio at the appropriate wavelength so that

$$P_m = P_{m'} \qquad \text{(IV-8)}$$

to a good approximation

4.2 Hanle Effect

4.2.1 Introduction to Hanle effect

In the geometry given in figure 32, we have the electron beam along the negative y-axis, the atomic beam along the x-

axis and the detected radiation along the Z-axis. So, the radiation can be considered to be coming from a dipole situated at the origin with componenents along the x, y, and z-axis . For unpolarised colliding partners , due to the cylindrical symmetry about the impact axis, one expects that the measured intensities of the radiation at angle 45° and 135° would be the same. This leads to $P_2 = P_3 = 0$, while the intensities polarised parallel and perpendicular to the impact axis are not equal, i.e., the Stokes parameter P_1 is not equal to zero.

The dipole and thus the measured polarisation may be affected by magnetic fields in the interaction region (Hanle 1924 , a translation of of the original articlewas made by Moruzzi 1991) . As also reported by Mitchell and Zemansk (1934) that Hanle made a thorough study of the polarisation of the mercury resonance line at 253.7nm in the presence of a weak magnetic field. Hanle applied the magnetic field in several directions and measured the polarisation of the emitted radiation. Of particular interest was the case when the direction of the applied magnetic field coincided with the direction along which he detected the emitted radiation. He found that, if the magnetic field was strong enough, the emitted radiation was totally unpolarised. By reducing the field little by little, the emitted radiation became more and more polarised reaching the maximum polarisation at zero field. This depolarisation of the emitted light due to the application of a magnetic field is known as Hanle effect. Even without magnetic field the polarizaion of the fluorescence radiation is not 100% if the excited state is affected by fine

struture or hyperfine structure interaction. Sodium and potassium both have fine and hyperfine structure. Theoretically the polarisation of the emitted radiation is therefore 12.9% at threshold (Percival and Seaton, 1958 and Kleinpoppen, 1969).

Using electron impact excitation the measured degree of polarisation for the sodium resonance lines 3P - 3S is 10% in a very weak field (Enemark and Gallagher 1972). For the potassium resonance lines (5P - 4S) a brief experiment was carried out to measure the linear polarisation parameter, P_1, as a function of the strength of the magnetic field near the threshold energy of 3.06eV for excitation of the states $5^2P_{3/2,1/2}$, and the results are shown in figure 33.

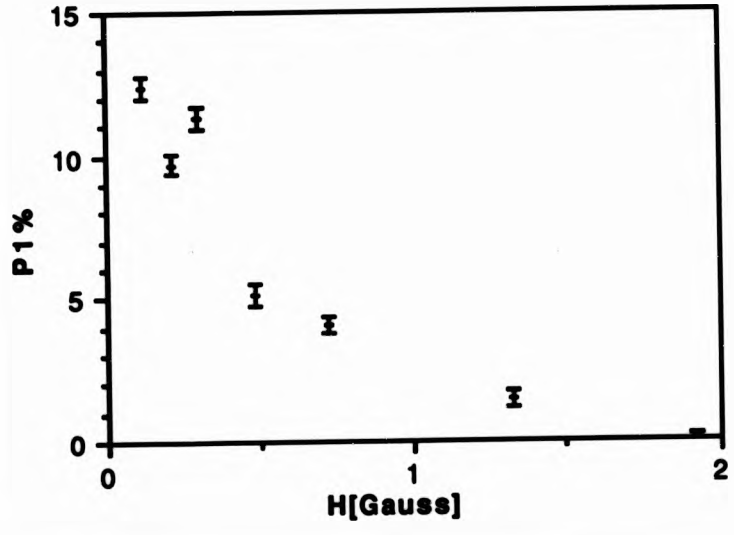

Fig 33 Measured variation in the polarisation parameter, P_1, of the potassium resonance line (5P-4S) as a consequence of the application of a magnetic field along the z-axis .

4.2.2 Classical Hanle effect theory

The classical theory of radiation can explain the Hanle effect . We follow the argument of Corney (1977) in explaining the Hanle effect. If the emitted radiation is polarised linearly and parallel to the impact axis (electron beam) it can be considered to be coming from a single damped oscillator which oscillates at an angular frequency ω_0. The electric field $\mathbf{E}(t)$ varies as

$$\mathbf{E}(t) = E(0) .\exp \{-i(\omega_0 - i\Gamma /2)(t-t_0)\}. \mathbf{i} \qquad \text{(IV-9)}$$

where $\Gamma = 1/\tau$ is the damping constant

and τ = radiative lifetime of the excited atom .

So, when we apply a finite magnetic field to this oscillating electron it will experience the Lorentz force

$$\mathbf{F} = -e\mathbf{v} \times \mathbf{B} \qquad \text{(IV-10)}$$

where $\mathbf{v}$ = velocity of the electron.

This Lorentz force will cause the oscillator to precess about the magnetic field with the Larmor frequency given by

$$\omega_L = g_F \frac{e}{2m} B = \frac{(g_F \mu_B B)}{\hbar} \qquad \text{(IV-11)}$$

where g_F is the Lande g-factor to be applied for the excited $3P_{3/2}$ state for sodium and the $5P_{3/2}$ state of potassium , respectively.

If we look towards the radiating atom, then it follows from IV-11 that by increasing the applied field more and more, the oscillation will be able to complete the rosette before its energy has been radiated away as shown in figure (34) and (35) , and consequently the emitted radiation suffers progressive depolarisation . For a weak magnetic field the oscillator will only be able to complete a small fraction of the rosette and the polarisation of the emitted radiation will only be slightly reduced (Fig. 35) . Actually ,the polarisation properties of the emitted light are not determined by the magnetic field alone but by a combination of the magnetic field and the lifetime of the excited state Thus an atom of shorter lifetime placed in a weak magnetic

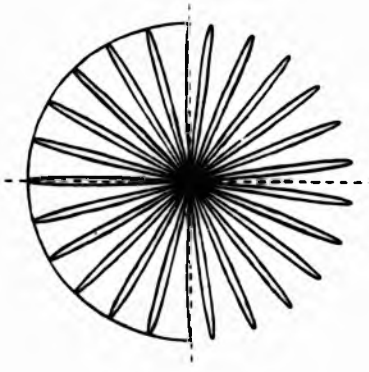

Fig. 34 Strong magnetic field or long lifetime

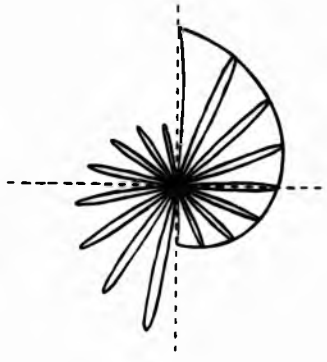

Fig. 35 Weak magneticfield or short lifetime

field (Fig.35) would emit more highly polarised light than an atom of longer lifetime placed in the same field (Fig.34).

The Hanle effect has therefore been widely used to measure lifetimes of excited states .

4.2.3 Fine and hyperfine structure of sodium and potassium

The alkali metal atoms such as sodium and potassium are composed of a single electron outside a core of completely filled electronic shells. This outer electron possesses an angular momentum, L, and an intrinsic angular momentum, S, coupled together to produce a multiple structure for each level (fine structure). The energy shift due to the spin orbit interaction is given by Weissbluth (1978).

$$E_{so} = \frac{Z^4 e^2 \hbar^2}{4a_0^3 m^2 c^2} \frac{J(J+1) - L(L+1) - S(S+1)}{n^3 (L+1)(L+\frac{1}{2})L} \qquad \text{(IV-12)}$$

where $a_0 = \hbar^2/me^2$ is the Bohr radius, m the rest mass of the electron and $J = L + S$ the total angular momentum. Since J is confined to the values $L \pm \frac{1}{2}$ and $S = \frac{1}{2}$ then

$$E_{so} = E_{L\pm\frac{1}{2}} = \frac{Z^4 e^2 \hbar^2}{2a_0^3 m^2 c^2} \frac{1}{n^3 (L+1)(L+\frac{1}{2})L} \cdot \begin{vmatrix} \frac{1}{2}L \\ -\frac{1}{2}(L+1) \end{vmatrix} . \qquad \text{(IV-13)}$$

So ,the splitting between $P_{3/2}$ and $P_{1/2}$ is given by

$$\delta E_{so} = 5.84 \frac{Z^4}{n^3 L(L+1)} \text{ cm}^{-1}$$

The P state splits as a result into two components as shown below

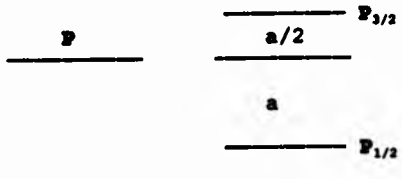

where the splitting $a \propto \frac{Z^4}{n^3 (L+1)(L+\frac{1}{2})L}$ (IV-14)

(Haken and Wolf, 1984)

Not only does the atom have an angular momentum L and spin S, but the nucleus also possesses a spin I, which couples with J to give the total angular momentum operator F such that

$$\mathbf{F} = \mathbf{I} + \mathbf{J}$$

$$\mathbf{J} = \mathbf{L} + \mathbf{S}$$

F takes the values

$$F = I + J,\ I + J - 1,\ \ldots\ldots\ |I-J|$$

since $I = 3/2$ for sodium and potassium there will be further splitting of the state into hyperfine structure , e.g. the ground states denoted by $3^2S_{\frac{1}{2}}$ and $4^2S_{1/2}$ will split into $F = 1$ and $F = 2$ states.

The general formula for calculating the hyperfine energy levels is given by Kopfermann (1958)

$$E = E_J + AC/2 + B\ \frac{3/4C(C+1) - I(I+1)J(J+1)}{2I(2I-1)J(2J-1)} \qquad \text{(IV-15)}$$

where E_J = energy of the multiplet level

$$C = F(F+1) - I(I+1) - J(J-1)$$

$$F = I+J,\ I+J-1,\ \ldots.|I-J| \qquad \text{(IV-16)}$$

The values for the relevant hyperfine structure constants A and B are listed in table 1 quoted by Happer (1975).

Figure 36 shows the hyperfine energy levels of ^{23}Na for the $3^2S_{1/2}$, $3^2P_{1/2}$ and $3^2P_{3/2}$ states .

Table 1. hyperfine structure constants A and B (Happer 1975)

Element	n	$A(n^2S_{1/2})$ MHz	$A(n^2P_{1/2})$ MHz	$A(n^2P_{3/2})$ MHz	$B(n^2P_{3/2})$ MHz
^{23}Na	3	885.82	94.30	18.65	2.82
^{39}K	4	230.85	28.85	6.09	2.77
	5		8.99	1.972	0.866
^{41}K	5			1.08	

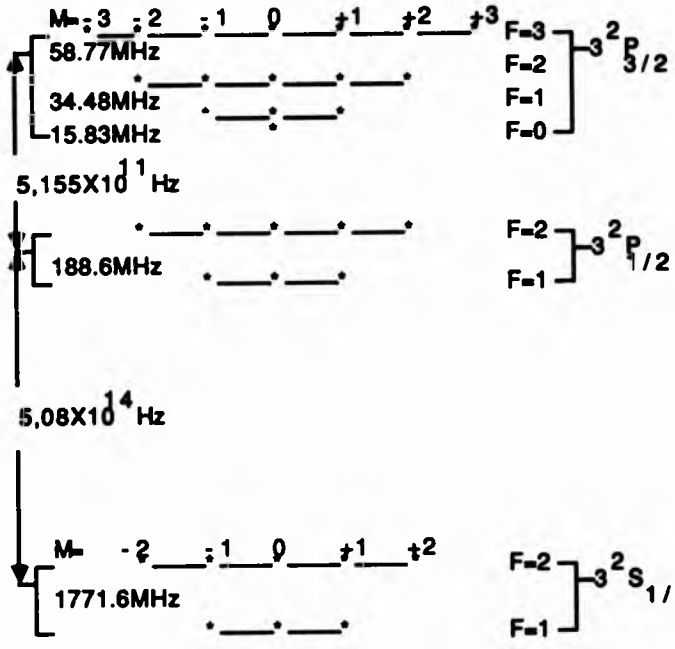

Fig 36 Hyperfine energy levels of ^{23}Na for $3^2S_{1/2}$, $3^2P_{1/2}$ and $3^2P_{3/2}$ states, indicating the hyperfine sublevels $|FM|$. Not to scale.

Figure 37 shows the hyperfine energy level of the $4^2S_{1/2}$, $5^2P_{1/2}$ and $5^2P_{3/2}$ of ^{39}K. The zero field hyperfine splittings for potassium are derived from the measured values in Table 1 and have the values given below :

For $J = \frac{1}{2}$ (ground state $4^2S_{\frac{1}{2}}$)

$E_{F=2} - E_{F=1} = 2A_{\frac{1}{2}} = 461.70$ MHZ

for $J = \frac{1}{2}$ excited state ($5^2P_{\frac{1}{2}}$)

$E_{F=2} - E_{F=1} = 2A_{\frac{1}{2}} = 17.98$ MHZ

and for $J = 3/2$ excited state ($5P_{3/2}$)

$E_{F=3} - E_{F=2} = 3A_{3/2} + B_{3/2} = 6.782$ MHZ

$E_{F=2} - E_{F=1} = 2A_{3/2} - B_{3/2} = 3.078$ MHZ

$E_{F=1} - E_{F=0} = A_{3/2} - B_{3/2} = 1.106$ MHZ

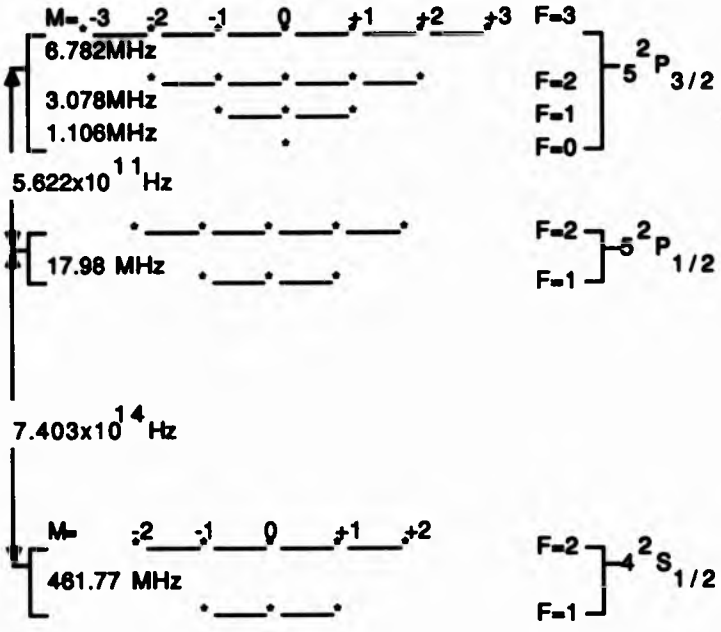

Fig 37 Hyperfine energy levels for the $4S_{\frac{1}{2}}$, $5P_{\frac{1}{2}}$ and $5P_{3/2}$ states of potassium (not to scale).

As discussed above both sodium and potassium have hyperfine structure. According to the theory of Percival and Seaton described by Kleinpoppen (1969) the linear polarisation of

the emitted radiation at threshold depends on two factors. One factor is the natural width of the excited state and the second is the fine and hyperfine structure. For an atom possessing no fine and hyperfine structure the level width can be ignored and at threshold the polarisation of the P-S fluorescence following a S-P excitation is 100%, because only the $m_l = 0$ substate is excited. The presence of fine structure reduces the polarisation at threshold especially when both $P_{3/2}$ and $P_{1/2}$ lines are observed. If the fine structure splitting is large compared to the natural width then the polarisation is 42.9%. When there is also a hyperfine structure splitting a further depolarisation occurs to the emitted radiation, depending on the value of the nuclear spin and the relation between lifetime and the hyperfine structure. In our case the nuclear spin, I, for both sodium and potassium is 3/2. In the case of the hyperfine structure splitting being large compared to the natural width of the state the polarisation will be 12.9% at threshold. The radiation will be depolarised further by the Hanle effect if the atoms are under the influence of a magnetic field.

4.2.4 Hanle effect depolarisation for the observed state

Figure 38 shows the experimental geometry of the interaction region. The free atomic beam is excited by the electron beam. The resultant resonance fluorescence light is collected and passed through the analyser and the interference filter to the photomultiplier. When the field is zero the $3P_{3/2}$ state

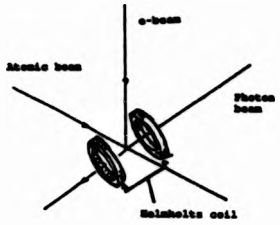

Fig. 38 Geometry of the interaction region

of sodium or $5P_{3/2}$ state of potassium is split into four hyperfine states of total angular momentum F.

$F = I + 3/2,\quad I + \tfrac{1}{2},\quad I - \tfrac{1}{2},\quad I - 3/2$

where I is the nuclear spin. In figure 39 we show the relative spacing of the levels for ^{23}Na and ^{39}K taken from Schmieder *et al* (1970).

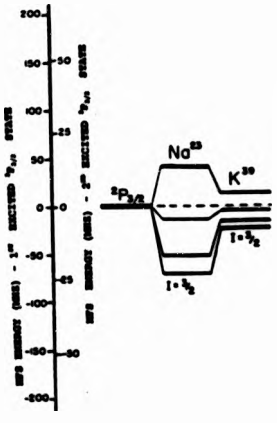

Fig. 39 Relative spacing of the hyperfine energy levels of the stable alkali atoms, ^{23}Na and ^{39}K for the $^2P_{3/2}$ states.

As the magnetic field increases above zero, the F states start to split into their Zeeman components. At low field each hfs level splits into (2F+1) equidistant levels and in total, there would be (2J+1)(2I+1) Zeeman levels for the complete hfs multiplet. The magnetic quantum number m_F can

take all the integer values between -F and +F. For a $^2P_{3/2}$ level at zero field there would be four hfs levels as seen in figure 39 (F=3, F=2, F=1 and F=0). By applying a weak magnetic field the F = 3 level will split into seven equidistant levels, the F = 2 level into five and the F = 1 level into three , while F =0 level will stay the same. The shift of the atomic hyperfine states in a weak magnetic field H_0 is given by Kopfermann (1958):

$$\Delta E_{F,m} = \mu_B m_F g_F H_0 \qquad \text{(I-17)}$$

where $$g_F = g_J \frac{F(F+1) + J(J+1) - I(I+1)}{2F(F+1)}$$

$$g_J = \frac{3J(J+1) + S(S+1) - L(L+1)}{2J(J+1)}$$

and μ_B = Bohr magneton

The energy difference between two adjacent levels is

$$\Delta(\Delta E_{F,m}) = \mu_B g_F \Delta m_F H_0$$

here $\Delta m_F = 1$ so

$$\Delta(\Delta E_{F,m}) = \mu_B g_F H_0$$

For the $^2P_{3/2}$ state we have I = J for sodium and potassium so

$$g_J = 4/3 \text{ and } g_F = 2/3$$

It follows that

$$\Delta(\Delta E_{F,m}) = h\nu = (2/3)\ \mu_B H_0 \qquad \text{(IV-18)}$$

ie $$\nu = \frac{(2/3)\ \mu_B H_0}{h}$$

where ν is the frequency corresponding to the energy difference $\Delta(\Delta E_{F,m})$.

The electron which is moving in its orbit, under the influence of the magnetic field will behave like a gyroscope and the oscillator will precess about the field H_0 with a frequency of approximately 1MHz for H_0 = 1 Gauss (see 4.2.2). In this case one precession, therefore, will take 10^{-6} sec. Since the lifetime of the $5^2P_{3/2}$ state of potassium is 140.8ns (Happer 1963) this means that during the lifetime the orbit will make 1/7 of a precession equivalent to 51°. This situation is unsatisfactory because it will reduce the linear polarisation, P_1, of the emitted radiation, to below its maximum possible value and as a consequence P_2 will not be zero anymore. Therefore the experiment on potassium was carried out at a field of 0.2 Gauss which means that the orbit will make (1/36) of a precession which is equivalent to only 10°. This setting of the field will not depolarise the emitted radiation by much and is still sufficient to maintain the spin orientation of the atomic beam .

For sodium the experiment was carried out at a field equal to 0.5 G. (which results in 1/60 of a precession in one life time, equivalent to 6°). We notice that the value of the linear polarisation is more sensitive to the applied magnetic field for the $5^2P_{3/2}$ state of potassium, than for the $3^2P_{3/2}$ state of sodium ; this is so because the lifetime of the $5^2P_{3/2}$ state of potassium is much larger than the lifetime of the $3^2P_{3/2}$ state of sodium.

4.3 MEASUREMENT AND DISCUSSION

4.3.1 Sodium Results

Figs. 40a&b show the linear polarisation of the sodium D lines ($3^2P_{3/2,1/2} - 3^2S_{1/2}$) as a function of the electron energy. The measurement was carried out under the influence of a weak magnetic field of 0.5G set parallel to the photon direction. The linear polarisation P_1 observed is shown in comparison with the previous measurement done by Osimitsch (1983) (Fig 40a) and Jitchin *et al* (1984) (Fig 40b). As we see from figure 40a&b , our measurement of P_1 for sodium is in good agreement with their results because P_1 is independent of the atomic beam polarisation. Also, figures 40a&b show the various theoretical calculations of the linear polarisation. The maximum value of P_1 occurs near the threshold wich is about 12%. As we can see the experimental and theoretical predictions of P_1 are in fairly good agreement at higher energy but at low energy the theoretical prediction is greater, which might be to some extent an effect of the energy width of the electron beam.

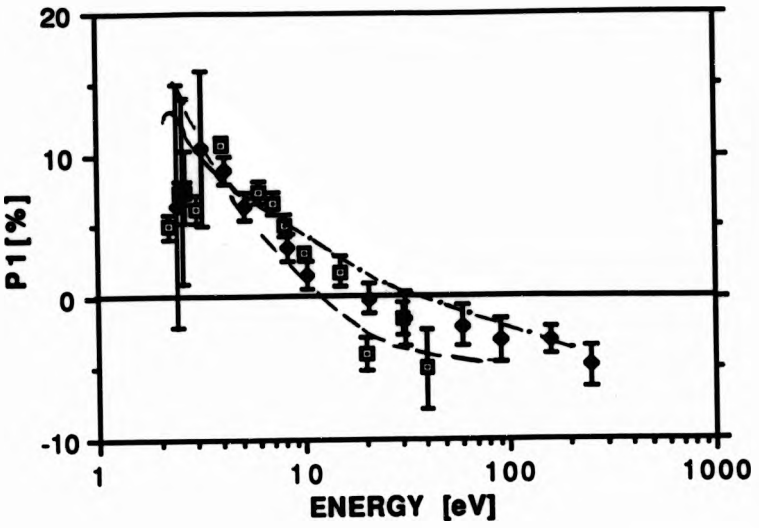

Fig. 40a The linear polarisation P_1 of the sodium D resonance lines. The Na atoms were polarised by magnetic-state selection in a hexapole magnet and excited by unpolarised electrons. Experimental data not corrected for cascades : □ , present work ; ♦ , Osimitsch (1983) . Theoretical curves:___, Moores and Norcross (1972); --- Tripathi (1973), exchange neglected; _.-._.-., Kennedy *et al* (1977).

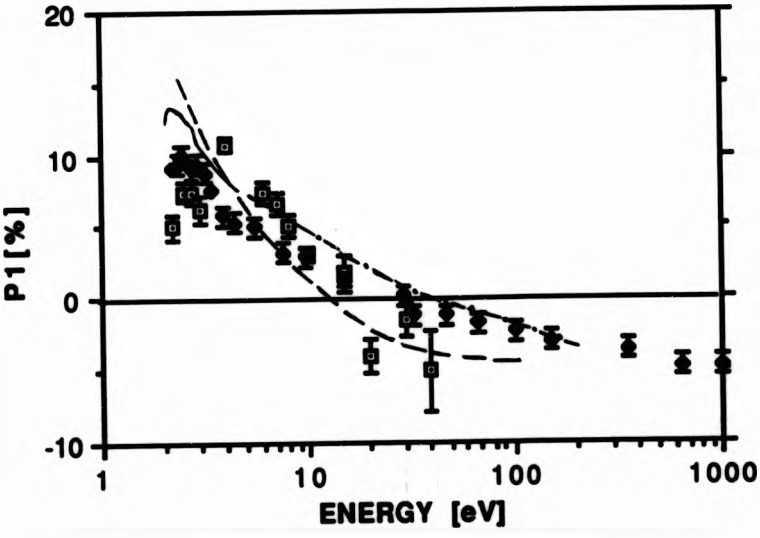

Fig (40b) AS Fig. 40a , showing measurement : □, present work and ♦ ,Jitschin *et al (1984)*.

Fig. 41, shows the linear polarisation parameter, P_2, of the sodium D-lines ($3^2P_{3/2,4} - 3^2S_4$). Theoretically the value of P_2 is zero, as indicated by the solid line in the figure provided the applied magnetic field in the interaction region is zero. For the magnetic field of 0.5G used in the experiment, P_2 should still be very close to zero and this is confirmed by the data in Fig 41. The average value of P_2 of our measurement is -0.03 ±1.30% and in the case of Osimitsch and Jitschin about 0.1 ± 1.7% and <1.5% respectively. All the three values are compatible with zero within the experimental errors.

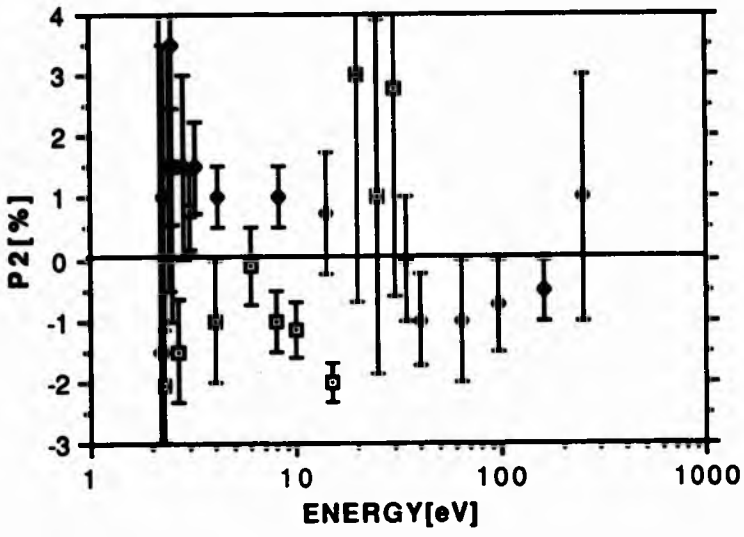

Fig (41) The linear polarisation, P_2, of the sodium D resonance line. The Na atoms were polarised by magnetic-state selection in a hexapole magnet and excited by unpolarised electrons. Experimental data: □, present work not corrected for Cascades, and ♦ , Osimitch (1983) ; ___, theoretical curve.

Figures 42 a and b show the circular polarisation, P_3, of the sodium resonance D-lines ($3^2P_{3/2,1/2} - 3^2S_{1/2}$) in comparison with theory and previous measurements by Osimitsch (1983) and Jitschin *et al* (1984). As we see from the figures the circular polarisation P_3 increases more or less steadily from its threshold value to reach a nearly constant value above 30eV. Our present measurements for the circular polarisation are consistently a little larger than the previous measurements, even though the atomic polarisation should be the same. Our results are in good agreement with the theoretical work by Moores and Norcross (1972) and Kennedy *et al* (1977). The reason for our circular polarisation P_3 being higher than the previous measurements may possibly be attributed to a better setting of the guiding field which would cause less depolarisation of the atomic beam on the way between the hexapole magnet and to the interaction region .

Figure 43 shows the circular polarisation P_3 of the D- lines as a function of the magnetic field at energy 25eV. The positive part of the polarisation is measured when the magnetic field is pointing towards the observer and the negative values are obtained when the direction of the magnetic field is away from the observer. The curve is fairly symmetric and reaches saturation at a magnetic field of about 0.5G. The curve being symmetric indicates that our experimental setting is reasonable . So we took our measurements for linear polarisation, P_1, P_2 and the circular polarisation P_3 at a magnetic field of 0.5G.

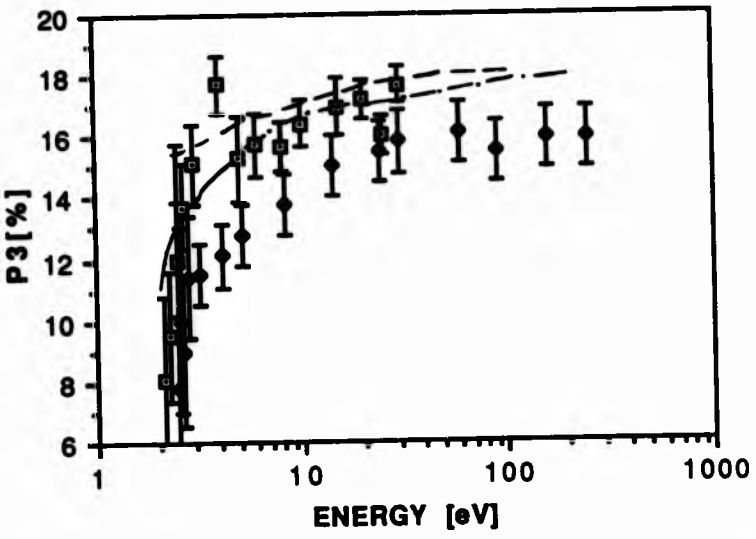

Fig. 42a Circular polarisation P_3 of the sodium D resonance lines. The Na atoms were polarised by magnetic state selection in a hexapole magnet. Experimental data; □ , present work .♦ , Osimitsch (1983) . Theoretical work has been calculated by Jitschin(1984) from the available information of ---Tripathi *et al* (1973), ___ Moores and Norcross (1972) -.-.- Kennedy *et al* (1977).

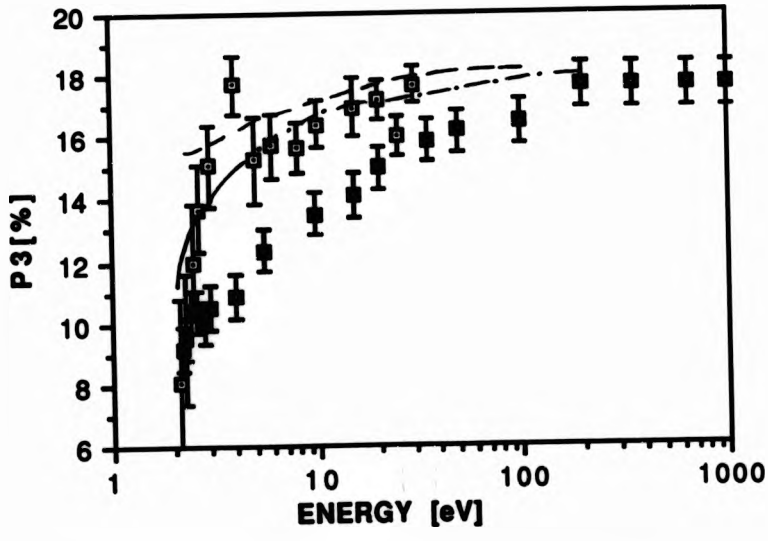

Fig. 42b As figure 42a , showing measturements: □ , present work.■ , Jitschin et al. (1984).

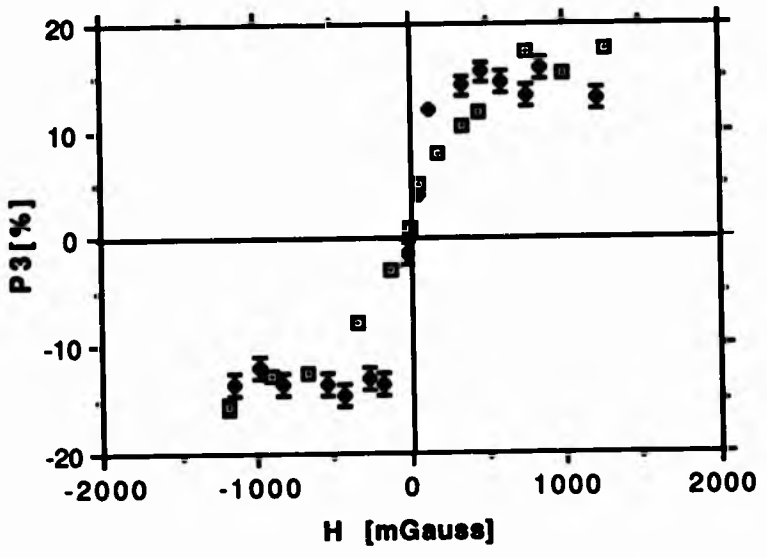

Fig. 43 Circular Polarisation P_3 as a function of the applied magnetic field, for the sodium resonance lines $3^2P_{3/2} - 3^2S_{1/2}$. The sodium atoms were polarised using a hexapole (P_1 = 21%). □, present work ,♦, Osimitsch (1983). Errors are too small to be shown

4.3.2 Potassium Results

When we measured the linear polarisation for potassium we were very careful with the magnetic field applied in the interaction region. As explained in 4.2.4 a magnetic field of 0.70G, should partially depolarise the fluorescent radiation so that P_1 will be reduced, while at the same time the linear polarisation, P_2, sould no longer be equal to zero. This is confirmed by the results shown in figure 44 where the linear polarisation, P_1, of the potassium resonance lines ($5^2P_{3/2,1/2} - 4^2S_{1/2}$) was taken with an applied magnetic field of 0.7G. The maximum value of P_1 in this field is in the neighbourhood of 4%.

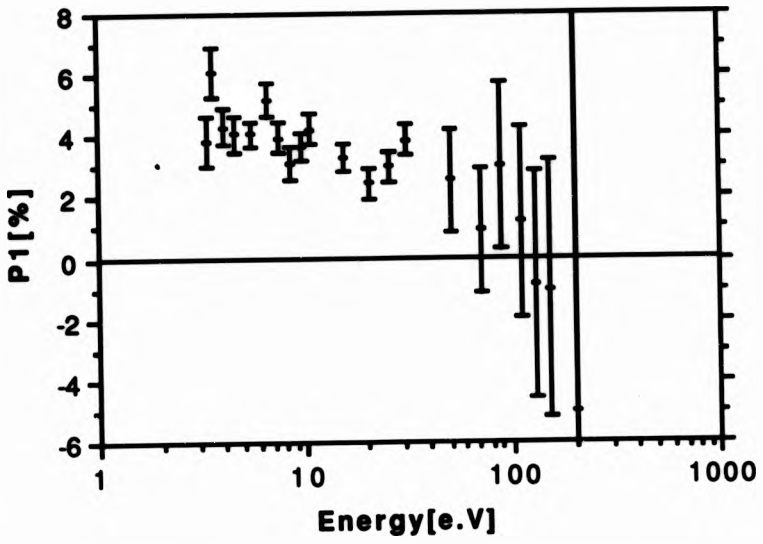

Fig. 44 The linear polarisation, P_1, of the potassium resonance lines $5^2P_{3/2,4} - 4^2S_{1/2}$. A magnetic field of 0.7Gauss is applied in the interaction region.

In contrast figure 45 shows the linear polarisation P_1 of the potassium resonance lines ($5^2P_{4,3/2} - {}^2S_4$) as a function of the electron energy taken at an applied magnetic field of 0.2G. We notice from the graph that at 3.3eV, which is close to the excitation threshold of the 5P level of potassium (3.06 eV), we obtain the maximum linear polarisation of about 10%. The polarisation decreases as the energy increases and changes sign at approximately 20eV. No other experimental or theoretical data are available for comparison . If we compare the potassium linear polarisation parameter P_1 in Fig. 45 with the corresponding sodium result in Fig. 40a,b we findstrong similarities of the values above approximately 5 eV including the sign change of P_1 at approximately 20 eV. However , near the threshold the behaviour appears to be

different , sodium showing a maximum of P_1 above threshold while P_1 for potassium apparently keeps increasing right down to the threshold energy.

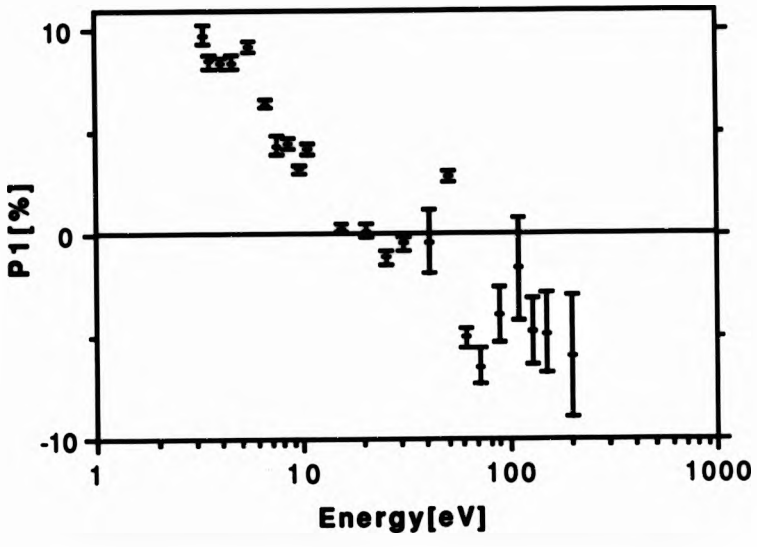

Fig. 45 The linear polarisation P_1 of the potassium resonance lines ($5^2P_{3/2,4} - 4^2S_4$) as a function of the electron energy. The applied magnetic field in the interaction region is 0.2G.

Figure 46 shows the linear polarisation P_2 for the potassium resonance lines ($5^2P_{4,3/2} - 4^2S_4$) measured with an external magnetic field of 0.2G. The average value of P_2 is 0.48 ± 1.13%

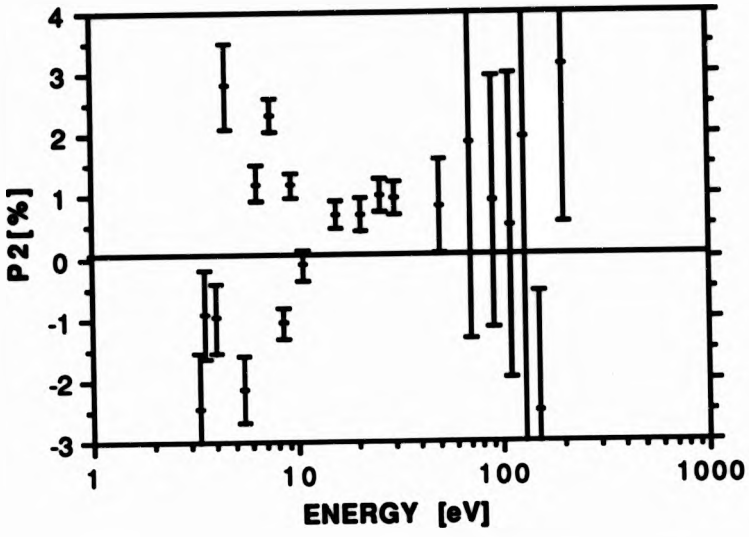

Fig. 46 The linear polarisation, P_2, of the potassium resonance lines ($5^2P_{4,3/2} - 4^2S_4$) as a function of the electron energy. The applied magnetic field is 0.2G.

Figure 47 shows the circular polarisation P_3 of the potassium resonance lines ($5^2P_{4,3/2} - 4^2S_4$) as a function of the electron energy. The trend of P_3 is similar to that observed for Na Fig. (42a&b), showing a rise of P_3 from 6.5% close to threshold to a nearly constant value of 16% above 25eV. There is an indication that there may be some structure at low energy. No other measurements or calculations are available for comparison. The large error bars at high energy are due to the generally low cross sections for thesecond resonance line 5P-4S compared with the first resonance line 4P-4S and the particularly steep decline of the 5P-4S cross section with increasing energy as shown in Fig 8.

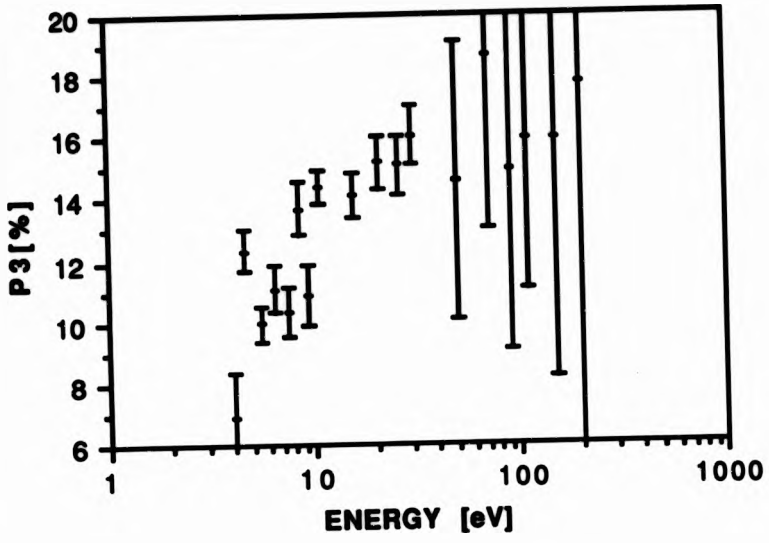

Fig. 47 The circular polarisation P_3 as a function of the electron energy for the potassium resonance lines $5^2P_{3/2,1/2} - 4^2S_{1/2}$. The potassium atoms were polarised by magnetic state selection in a hexapole magnet, P =21%.

Figure 48 shows the circular polarisation P_3 of the resonance lines $5^2P_{3/2,1/2} - 4^2S_{1/2}$ as a function of the applied magnetic field in the direction of observation and in the reverse direction. The electron energy is 25eV. The curve is fairly symmetric and reaches saturation at 0.2G. The curve, being symmetric, indicates that our experimental setting is correct. All our final polarisation measurements for potassium were carried at 0.2G .

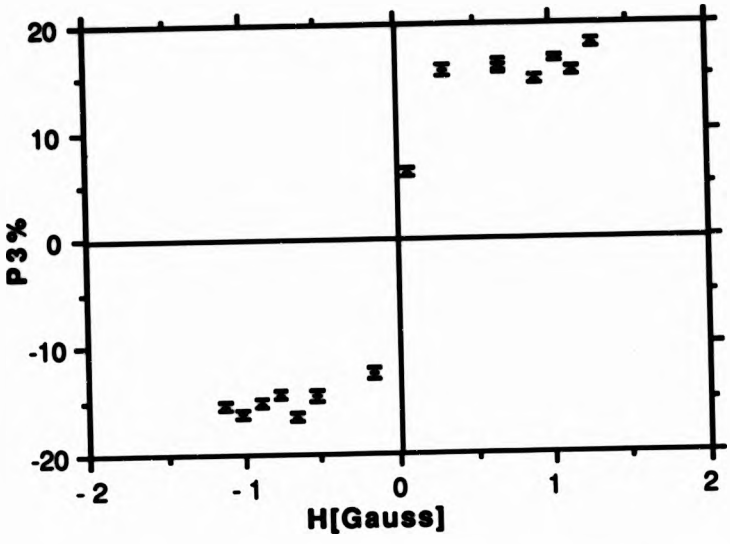

Fig .48 . The circular polarisation P_3 of the resonance radiation $5^2P_{4,3/2} - 4^2S_4$ of potassium as afunction of the applied magnetic field . The potassium beam was polarised (P_A =21 %) using a hexapole magnetic field .

CHAPTER V

5 CONCLUSION AND SUMMARY

From the experiment we have done on sodium and potassium, three main conclusions can be drawn concerning P_1, P_2 and P_3.

To start with we can say with confidence that the linear polarisation P_2 is zero within the limits of experimental error for sodium and potassium. The average value of P_2 for sodium is $(-0.03 \pm 1.30)\%$ and for potassium $(0.48 \pm 1.16)\%$. The circular polarisation, P_3, was measured at a magnetic field of 0.5G for sodium and 0.2G for potassium. At low energy, the measured circular polarisation is relatively low (about 7%) for both sodium and potassium. This low value of P_3 reveals some of the details of the processes which are going on when a low energy electron interacts with the polarised sodium and potassium atoms. At low energy the three interaction channels, exchange ,direct and mixed are comparable in magnitude and this leads to a low value of the circular polarisation P_3 due to spin flip of the electron of the atom in the exchange process. At higher energy the circular polarisation reaches about 17% for both sodium and potassium which indicates that the contribution of the exchange process is minimal at high energy .

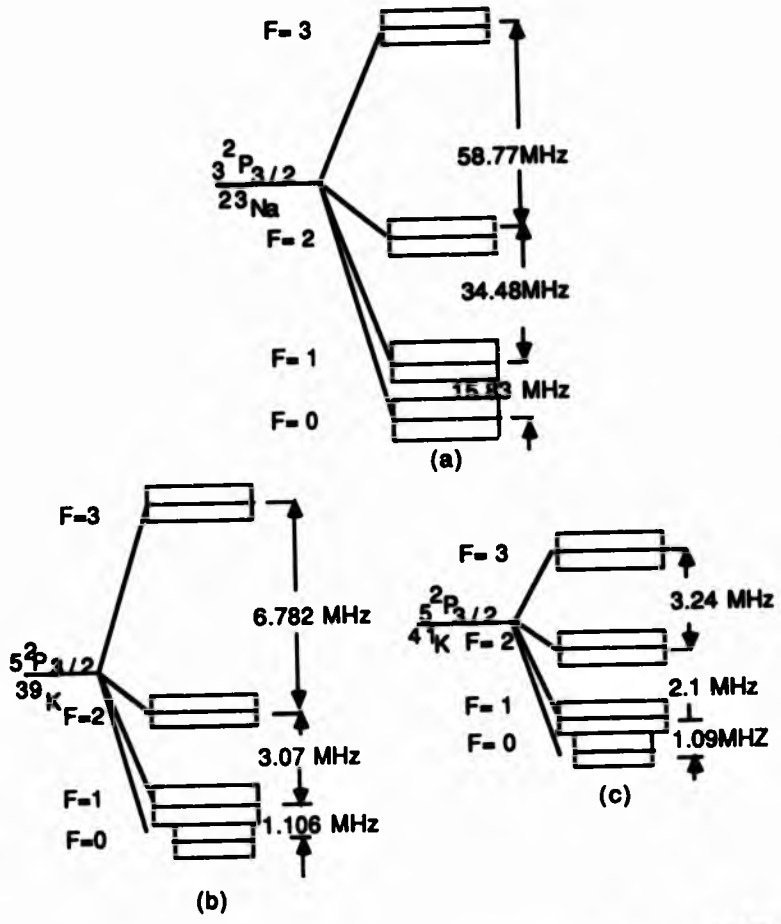

Fig (49) The hyperfine splitting of the $3^2P_{3/2}$ state of sodium (a) and the $5^2P_{3/2}$ states of the isotopes 39 (b) and 41 (c) of potassium. The level widths are also shown (Happer, 1975)

In Figure 49 we show the energy level diagrams and natural level widths for the excited $P_{3/2}$ states of the sodium and potassium atom. The potassium metal actually consists of 6.9% ^{41}K and 93.1%

^{39}K , and both cases are shown. For sodium the natural level width is 9.95 MHz (τ=16.0 nsec , Schmieder *et al* ,1970) , while for potassium, it is 1.13 MHz (τ=140.8 nsec ,Schmieder *et al* ,1968) . As we see from Figure 49a the level width is noticeably smaller than the fine and hyperfine splitting in the case of sodium . A threshold polarisation P_1 of 12.9% is therefore expected which our measurements (Fig. 40 a&b) did not obtain ,possibly due to resonances near threshold. However, the maximum measured polarisation occurs in the neighbourhood of the threshold and is about 12%. For ^{39}K (Fig 49b) we notice that the splitting of the $P_{3/2}$ state is still larger than the level width except for the F=1 and F=0 states for which the level width is comparable to the splitting. This will probably only lead to a marginal increase of the threshold polarisation beyond 12.9%. We have measured about 13.2% as can be concluded from figure 33 . This value is unlikely to be affected very much by the 6.9% abundance of^{41}K whose hyperfine splitting is less than that of ^{39}K but still only leading to a slight overlap between F=1 and F=0 as indicated in Fig 49c .

Finally , we would suggest to extend these measurements into a systematic study of the alkali atoms by the same method to Rb and Cs .

BIBLIOGRAPHY

Barnes L L Lane, N F and Lin C C (1965) Phys.Rev. **A137** 388.

Bartschat K and Blum K (1982) Z. Phys. Atoms and Nuclei **304** 85-88 .

Bartschat K ,Blum K ,Hanne G F and Kessler J (1981) J . Phys. B: At. Mol. Phys. **14** 3761 .

Baum G Moede M Raith W and Schröder W (1983) Proc. **13th** Conf. on the Phys of Elec. and Atomic Collisions ,Berlin ed. by Eichler J et al, 144.

Blum K (1981) Density Matrix theory and application (Plemum Press, New York).

Blum K and Kleinpoppen H (1979) Phys. Rep. **52** 203.

Born M and Wolf E (1970) Principal of Optics (New York, Pergamon Press).

Bransden B H and McDowell M R (1977) Phys. Rep.**30c** 209.

Bransden B H and McDowell M R (1977) Phys. Rep. **46** 251.

Briggs J and Anderson N (1988) Fundamental processes of atomic dynamics (Plemun Press, New York)313.

Burke P G and Schey H (1962) Phys. Rev. **A126** 163.

Campbell D M Brash H M and Farago P S (1971) Phys. Lett.**6** 449 .

Chen S T and Gallagher A (1976) Phys. Rev. **A14** 593 .

Chen S T and Gallagher A C (1978) Phys. Rev **A7** 551.

Corney A (1977) Atomic and Laser Spectroscopy (Clarendon Press Oxford) 473 .

Drukarev G F (1987) Collision of eletrons with atoms and molecules (Plenum Press, New York) 76.

Edmonds A R (1959) Angular Momentum in Quantum mechanic (NJ:princeton University press).

Felden M M and Felden M A (1973) Can. Phys.**51** 1709.

Ehlers V J and Gallagher A (1973) Phys. Rev. **A7** 1573 .

Enemark E A and Gallagher A C (1972) Phys Rev. **A6** 192.

Esterman I (1946) Rev. Mod Phys. **18** 300 .

Flower D R and Seaton M J (1967) Proc. Phys. Soc. (London) 91 59 .

Firester A H (1966) Rev. Sci Inst. 37 1264 .

Friedburg H (1951) Z. Phys. 130 493 .

Green T J and and Williamson Jr W (1974) At. Data Nucl. Data Tabls 14 16 .

Hafner H Kleinpoppen H and Kruger H (1965) Phys. Lett. 1 270 .

Haken H and Wolf H C (1984) Atomic and Quantum Physics (Springer-Verlag, Berlin) .

Handbook of Physics (1967) (Mc Graw Hill) 6-138 .

Hanle W (1942) Z.Phys. 30 93 .

Happer W (1975) Atomic Physics 4 (Plenum Press, New York) 651.

Heddle D and Gallagher J W (1989) Rev. Mod. Phys. 61 221.

Hils D (1971) Ph.D thesis University of Colarado (1971).

Hils D Jitschin W and Kleinpoppen H (1981) Appl.Phys. 25 39.

Hughes V W Long R L ,Lubell M S ,Posner M and Raith W (1972) Phys. Rev.A5 ,195 .

Jitchin W (1989) J Phys. B: At. Mol. Phys. 17 1899 .

Jitschin W, Osimitsch S, Reihe H, Kleinpoppen H, and Lutz H (1984) J Phys B: At. Mol. Phys. 17, 1899 .

Karule E M and Peterkop R K (1965) Atomic Collision III Akad. Nauk.Latv. SSR Ins. Fiz.,V.ya. Velder,Ed.,Riga,3.

Karule E M and Peterkop R K in Atomic ollision Iv edetted by V .Ia.Veldre,Available through SLA Translational Service, John Crear Library,86E.Randolph,Chicago,III,Translation no. TT-66-1239

Kennedy J V, Myerscough V P and McDowell M R (1977) J.Phys. B:At. Mol. Phys. 10 , 3759.

Kleinpoppen H (1969) Physic of one or two electron atoms (North-Holland) 612 .

Kleinpoppen H (1971) Phys. Rev A3, 2015.

Kopfermann H and Schneider E (1975) Nuclear moments (Academic Press, New York) 651.

Korff D (1973) PhD Dissertationu Uiversity of Wisconsin.

Lane N F and Lin C C (1964) Phys. Rev.A9 47.

Martin W L S and Engel A V (1977) J.Phys. D. Appl.Phys. 10 863.

Math Cad 2.52 , (1986--1989) ,Mathsoft Inc. .

Mathur K C, Tripathi A N and John S K.(1969) Chem.Phys.51 2980.

McCavert P and Rudge M R H (1972) J.Phys. B: At. and Mol. Phys.5 508.

McGregor I (1979) PhD thesis University of Stirling .

Melissa L and Moody S E (1977) Rev. Sci Inst. 48 131.

Mitchell A C G and Zemansky M W (1934) Resonance Radiation and excited atoms (the Cambridge series of Physical Chemistry) 258 .

Moisewitch B L and Smith S J (1968),(1969) Rev. Mod. Phys.140,238

Moisewitch B L and Smith S J (1969) Rev. Mod. Phys.140,Err.

Moorse D L and Norcross D W (1972) J.Phys B: At. and Mol. Phys. 5 1482.

Moorse D L (1976) J.Phys. B: At. and Mol.9 ,1329.

Moruzzi M (1991) ,The Hanle effect and level crossing spectroscopy ed. Moruzzi G and Strumia F (New York , Plenum Press) 34-46.

Osimitsch S (1983) Diplomarbeit., Universität Bielefeld.

Papp F F,Omanjuk N and Shpenik C B (1983) in ICPEAC XIII: Abstracts of Contributed Papers of the XIIIth ICPEAC ,(Berlin, West Germany , July & August (1983) 744.

Percival I C and Seaton M (1958) J.Phil Trans. R.Soc. A251 113.

Phelps J O, Solomon J E, Korff D F and Lin C (1979) Phys. Rev. A20 1418 .

Phelps E A and Lin C (1981) Phys. Rev. A 24 1299.

Ramsey N F (1956) Molecular Beams (Oxford Press) .

Rubin K, Perel J and Bederson B (1960) Phys.Rev 117 151.

Salmona A and Seaton M J (1961) Proc. Phys. Soc. (London)77 619.

Seaton M J (1962) Proc. Phys. Soc. (London) 79 1105.

Schmieder R W ,Lurio A ,Happer W and Khadjavi A Phys. Rev. A 2 1216

Schmieder R W ,Lurio A ,Happer W and Phys. Rev. A173 76

Schröder W (1982) PhD thesis Universität Bielefeld .

Simpson J A and Kuyatt C E (1963) J.Research of National Buareau of Standards 67C 279 .

Simpson J A (1967) Methods of Experimental Phys. 4 part A. Atomic and Electron Physics, Atomic sources and Detectors 84 .

Simpson J A and Kuyatt C E (1963) Rev. Sci.Ins. 34 265.

Tripathi A N and Mathur K J (1973) J. Phys. B: At. and Mol.Phys 6 1431 .

Vainshtein L A (1969) Opt. Spectrosc. 18 947.

Vainshtein L A (1965) Opt. Spectrosc. 18 538.

Walters H R (1973) J.Phys. B: At. and Mol. Phys. 6 1003.

Weissbluth M (1978) Atoms and Molecules (N.Y.:Academic Press) 340.

William W and Trajmar S (1977) J.Phys. B:At. and Mol. Phys. 9 1529.

Zapesochny I P, Postoi E N and Alekshakin I S (1975) Sov. Phys.JETP 41 865.

APPENDIX

Data for Figure 22 (Na)

Detector distance (cm)	I(Na^+ current) (nA)
0.2	5.4
0.4	6.0
0.6	6.6
0.8	8.4
1.0	11.0
1.2	14.0
1.4	14.8
1.6	14.8
1.7	14.3
2.0	10.2
2.2	8.0
2.4	6.7
2.6	6.3
2.8	6.1
3.0	5.8
3.2	5.7
3.3	5.6

Data for Figure 23 (K)

Detector distance	I(K^+ current) (nA)
0.0	1.6
0.2	2.0
0.4	2.4
0.6	3.0
0.7	4.0
0.8	5.0
0.9	7.4
1.0	9.0
1.1	10.5
1.2	12.0
1.3	13.5
1.4	14.0
1.5	13.5
1.6	12.5
1.7	11.5
1.9	8.5
2.0	6.5
2.1	5.0
2.2	3.8
2.3	3.5
2.4	3.0
2.5	2.5
2.6	2.3
2.7	2.1
2.8	1.9
2.9	1.8
3.0	1.7

Data for Figure 29 (K)

Electron energy (eV)	Counts in 400 sec
3.5	322
5	1897
6	7953
7	18271
9	32868
10	72939
15	91800
20	129744
25	190026
30	15800

Data for Figure 18 (K)

Detector distance (cm)	I (K^+ current) (nA)
0.0	0.085
0.1	0.09
0.15	0.094
0.2	0.096
0.25	0.096
0.3	0.1
0.35	0.105
0.4	0.116
0.45	0.132
0.5	0.15
0.55	0.183
0.6	0.2
0.65	0.182
0.7	0.17
0.75	0.155
0.8	0.14
0.85	0.122
0.9	0.11
0.95	0.105
1.0	0.105
1.05	0.105

Detector distance (cm)	I (K^+ current) (nA)
0.0	0.122
0.1	0.125
0.15	0.128
0.2	0.128
0.25	0.126
0.3	0.125
0.35	0.129
0.4	0.136
0.45	0.145
0.5	0.154
0.55	0.16
0.6	0.166
0.65	0.173
0.75	0.18
0.8	0.196
0.85	0.196
0.9	0.186
0.95	0.166
1.0	0.150
1.05	0.138
1.1	0.13
1.15	0.126
1.2	0.126
1.25	0.125

Data for Figure 40a&b

P_1 Vs E (Ma)

Energy [ev]	P1[%]
2.1	5.66 ± 2.33
2.2	5.00 ± 0.78
2.5	7.50 ± 0.61
2.7	7.40 ± 0.70
3.0	6.30 ± 1.00
4.0	10.78 ± 0.47
6.0	7.45 ± 0.72
7.0	6.69 ± 0.77
8.0	5.11 ± 0.77
10.0	3.11 ± 0.52
15.0	1.90 ± 1.10
20.0	-4.00 ± 1.20
30.0	-1.50 ± 1.20
40.0	-5.00 ± 2.80

Data for Figure 41

P_2 Vs E (Ma)

Energy [ev]	P2[%]
2.3	-2.04 ± 0.90
2.5	1.52 ± 0.94
2.7	-1.50 ± 2.33
3.0	0.81 ± 2.33
4.0	-1.00 ± 2.33
6.0	-0.10 ± 2.33
8.0	-1.00 ± 2.33
10.0	-1.13 ± 2.33
15.0	-2.00 ± 2.33
20.0	3.00 ± 2.33
25.0	1.02 ± 2.33
30.0	2.80 ± 2.33

Data for Figure 42a&b

P_3 Vs E (Ma)

Energy [eV]	P3[%]
2.1	8.11 ± 2.72
2.3	9.50 ± 2.11
2.5	11.99 ± 1.88
2.7	13.70 ± 1.40
3.0	15.10 ± 1.30
4.0	17.72 ± 0.96
5.0	15.27 ± 1.43
6.0	15.71 ± 1.00
8.0	15.65 ± 0.82
10.0	16.39 ± 0.77
15.0	16.97 ± 0.95
20.0	17.20 ± 0.62
25.0	16.03 ± 0.62
30.0	17.8 ± 2.20

Data for Figure 43

P_3 Vs H (Ma)

H.[m.G.]	P3[%]
0.0	1.02 ± 0.31
50.0	5.08 ± 0.40
175.0	7.83 ± 0.41
350.0	10.47 ± 0.38
450.0	11.82 ± 0.41
770.0	17.46 ± 0.40
1000.0	15.32 ± 0.40
1288.0	17.71 ± 0.38
-130.0	-3.01 ± 0.44
-350.0	-7.77 ± 0.47
-680.0	-12.40 ± 0.52
-900.0	-12.66 ± 0.49
-1180.0	-15.60 ± 0.70

Data for Figure 33
P_1 Vs H (K)

H[G]	P1[%]
0.120	12.40 ± 0.38
0.216	9.78 ± 0.33
0.300	11.32 ± 0.41
0.480	5.09 ± 0.39
0.720	4.09 ± 0.28
1.320	1.47 ± 0.30
1.920	0.13 ± 0.10

Data for Figure 44
P_1 Vs E [H=.67Gauss] (K)

Energy [eV]	P2[%]
3.3	3.81 ± 0.82
3.5	6.13 ± 0.80
4.0	4.34 ± 0.62
4.5	4.09 ± 0.58
5.5	4.09 ± 0.42
6.5	5.20 ± 0.51
7.5	3.98 ± 0.54
8.5	3.15 ± 0.53
9.5	3.67 ± 0.49
10.5	4.23 ± 0.49
15.5	3.30 ± 0.48
20.5	2.46 ± 0.49
25.5	3.01 ± 0.50
30.5	3.88 ± 0.49
50.5	2.55 ± 1.66
70.5	0.92 ± 2.00
90.5	3.03 ± 2.67
110.5	1.19 ± 3.13
130.5	-0.88 ± 3.72
150.5	-1.00 ± 4.19
200.0	-5.03 ±13.47

Data for Figure 45
P_1 Vs E (0.2G) (K)

E. [eV]	P1[%]
3.3	9.82 ± 0.44
3.5	8.53 ± 0.33
4.0	8.42 ± 0.29
4.5	8.45 ± 0.33
5.5	9.21 ± 0.24
6.5	6.45 ± 0.16
7.5	4.42 ± 0.46
8.5	4.52 ± 0.23
9.5	3.24 ± 0.21
10.5	4.20 ± 0.26
15.5	0.36 ± 0.20
20.5	0.22 ± 0.29
25.5	-1.07 ± 0.34
30.5	-0.44 ± 0.36
40.5	-0.32 ± 1.50
50.5	2.89 ± 0.23
60.5	-5.04 ± 0.52
70.5	-6.42 ± 0.89
90.5	-3.91 ± 1.33
110.5	-1.65 ± 2.55
130.5	-4.75 ± 1.65
150.5	-4.81 ± 1.99
200.5	-5.98 ± 3.00

Data for Figure 46
P_2 Vs E (.2G) (K)

E. (eV)	P2[%]
3.3	-2.46 ± 0.92
3.5	-0.92 ± 0.72
4.0	-0.99 ± 0.58
4.5	2.81 ± 0.70
5.5	-2.14 ± 0.56
6.5	1.22 ± 0.29
7.5	2.32 ± 0.26
8.5	-1.07 ± 0.24
9.5	1.18 ± 0.21
10.5	-0.13 ± 0.24
15.5	0.72 ± 0.23
20.5	0.69 ± 0.27
25.5	1.00 ± 0.27
30.5	0.97 ± 0.26
50.5	0.85 ± 0.76
70.5	1.86 ± 3.18
90.5	0.91 ± 2.06
110.5	0.53 ± 2.48
130.5	1.96 ± 5.04
150.5	-2.49 ± 1.91
200.0	3.15 ± 2.56

Data for Figure 47

P_3 Vs E. (K)

E. [eV]	P3[%]
4.0	6.93 ± 1.44
4.5	12.35 ± 0.67
5.5	9.94 ± 0.56
6.5	11.10 ± 0.76
7.5	10.34 ± 0.81
8.5	13.71 ± 0.86
9.5	10.91 ± 1.00
10.5	14.42 ± 0.56
15.5	14.15 ± 0.73
20.5	15.18 ± 0.83
25.5	15.08 ± 0.96
30.5	16.04 ± 0.95
50.5	14.59 ± 4.53
70.5	18.65 ± 5.63
90.5	14.90 ± 5.84
110.5	15.98 ± 4.94
150.5	15.96 ± 7.79
200.5	17.77 ± 13.50

Data for Figure 46

P_3 Vs H [H=0.2 G] (K)

H[G.]	P3[%]
0.07	6.19 ± 0.47
0.31	15.71 ± 0.49
-0.17	-12.42 ± 0.49
-0.53	-14.63 ± 0.52
0.67	16.06 ± 0.60
0.67	15.88 ± 0.26
-0.65	-16.58 ± 0.33
-0.77	-14.47 ± 0.34
0.91	14.64 ± 0.33
1.03	16.58 ± 0.26
-0.89	-15.25 ± 0.34
-1.01	-16.23 ± 0.37
1.15	15.46 ± 0.29
1.27	17.98 ± 0.37
-1.13	-15.49 ± 0.32